Indisulam targets RNA splicing and metabolism to serve as a novel therapeutic strategy for high-risk neuroblastoma

Anke Nijhuis[1$], Arti Sikka[1$], Orli Yogev[2$], Lili Herendi[1], Clare Eckold[1], Gabriel Valbuena[1], Yusong Liu[1], Eirini Kouloura[1], Evon Poon[2], Barbara Martins da Costa[2], Adrian Benito[1], Holger Kramer[3], Alex Montoya[3], David Carling[3], Elizabeth J. Want[4], Yann Jamin[5], Louis Chesler[2] and Hector C. Keun[1,4*]

[1]Department of Surgery & Cancer, Imperial College London, London, UK [2]Division of Clinical Studies, The Institute of Cancer Research, London, UK. [3]Biological Mass Spectrometry and Proteomics Facility, Medical Research Council London Institute of Medical Science, London, UK [4]Department of Metabolism, Digestion and Reproduction, Imperial College London, London, UK. [5]Division of Radiotherapy and Imaging, The Institute of Cancer Research, London and Royal Marsden NHS Trust, UK.

[$]These authors contributed equally to this manuscript, listed alphabetically.

[*]Corresponding author, h.keun@imperial.ac.uk

Key words: neuroblastoma, RBM39, indisulam, spliceosome, drug repurposing, cancer metabolism

Abstract

Neuroblastoma is the most common solid tumour in childhood and prognosis remains poor for high-risk cases despite the use of multimodal treatment. Analysis of public drug sensitivity data showed neuroblastoma lines to be particularly sensitive to indisulam, a molecular glue that selectively targets RNA splicing factor RBM39 for proteosomal degradation via DCAF15-E3-ubiquitin ligase. In neuroblastoma models, indisulam induced rapid loss of RBM39, accumulation of splicing errors and growth inhibition in a DCAF15-dependent manner. Integrative analysis of RNAseq and proteomics data highlighted a distinct disruption to cell cycle and metabolism. Metabolic profiling demonstrated metabolome perturbations and mitochondrial dysfunction resulting from indisulam. Complete tumour without relapse was observed in both xenografts and the Th-*MYCN* transgenic model of neuroblastoma after indisulam treatment, with RBM39 loss confirmed *in vivo*. Our data imply

that dual targeting of metabolism and RNA splicing with anti-cancer sulphonamides such as indisulam is a promising therapeutic approach for high-risk neuroblastoma.

Introduction

Neuroblastoma is the most common solid and extra-cranial paediatric tumour, originating from neural crest cells of the sympathetic ganglia. Treatment options include surgical resection, cytotoxic chemotherapy, radiotherapy, myeloablative autologous stem cell transplantation and multimodal therapy. However, the prognosis for high-risk cases remains poor with a high incidence of tumour relapse [1]. Most high-risk cases are characterized by MYCN-amplification which accounts for 20% of all neuroblastoma cases [2].

Indisulam (E7070) is one of a class of aryl sulphonamides originally discovered by Eisai through several screens for small molecule inhibitors that block cell cycle progression [3, 4]. Thereafter, studies revealed that indisulam targets multiple checkpoints through G1 and G2 phases of the cell cycle, and disturbs and downregulates cyclin A, cyclin B, CDK2 and CDC2 via p21/p53 dependent mechanisms [5]. Tumour regression in HCT116 xenografts by indisulam was superior to other anti-cancer compounds such as 5-FU and Irinotecan [6], which prompted the investigation of indisulam in Phase I/II clinical trials as an anticancer agent for several advanced solid tumours [7-13]. Despite acceptable toxicity profiles, clinical responses have been modest and the efficacy of indisulam has never been tested in neuroblastoma.

More recently, the precise molecular mechanism of action for indisulam was uncovered by two independent studies [14, 15]. Indisulam binds to and induces a ternary protein complex between RNA Binding Motif 39 (RBM39) and the E3 ubiquitin ligase receptor DDB1 and CUL4 Associated Factor 15 (DCAF15) resulting in rapid proteasomal degradation of RBM39, aberrant RNA splicing and cell death [14, 15]. DCAF15 expression was shown to be necessary for this mode of action and thus proposed as a stratification marker of response in haematopoietic malignancies [14]. RBM39 is an SR-rich protein homologous to, and associated with, the key splicing factors U2 auxiliary factor 65 (U2AF65) [16, 17] and SF3b155 [18]. RBM39 has been proposed to serve as a pre-mRNA splicing factor [16, 19, 20] and loss of RBM39 causes alternative splicing defects [21]. Additionally, RBM39 is known to be a coactivator of transcription factors such as AP-1 and Estrogen Receptors (ER)

alpha and beta [20] and may also regulate metabolism via activation of the NF-κB/c-Myc pathway [22].

In this study, we demonstrate for the first time that indisulam is an effective anti-cancer agent in models of neuroblastoma. Indisulam reduced cellular growth and induced apoptosis *in vitro* and caused complete remission of tumours in two *in vivo* models of neuroblastoma. Indisulam results in DCAF15-dependent RBM39 degradation leading to splicing errors and reduced levels of proteins involved in cell cycle and metabolism. Consistent metabolic responses to indisulam were observed both *in vitro* and *in vivo*. In conclusion, our findings suggest that high-risk neuroblastoma may be particularly sensitive to the selective loss of RBM39 and modulation of splicing and metabolism by indisulam.

Materials & Methods

Cell Culture. IMR-32 cell line was purchased from the American Type Culture Collection (ATCC) (Manassas, VA). LS, SHEP and KELLY were obtained from the German Collection of Microorganisms and Cell Culture (DSMZ). All cell lines were maintained in ATCC's Eagle's Minimum Essential Medium (EMEM), supplemented with 10% foetal bovine serum (FBS) and 1% penicillin/streptomycin for routine culture. Cell lines were authenticated using short-tandem repeat DNA profiling by Public Health England and mycoplasma tested regularly.

2-D Growth and viability assays. Indisulam (E7070) was purchased from Sigma-Aldrich. Cells were counted at 72 hours with a trypan blue exclusion method using a haemocytometer or a Vi-CELL XR Cell Counter & Viability Analyser (Beckman Coulter). Cell viability was determined using the Vi-CELL XR analyser.

***In vivo* experiments**. All experimental protocols were approved and monitored by The Institute of Cancer Research Animal Welfare and Ethical Review Body (PPL no. 70/7945, later PPL P91E52C32), in compliance with the UK Home Office Animals (Scientific Procedures) Act 1986, the United Kingdom National Cancer Research Institute guidelines for the welfare of animals in cancer research [23] and the ARRIVE guidelines [24].

In vivo tumor xenograft of IMR-32 neuroblastoma cells

NCr-Foxn1^{nu} mice were injected subcutaneously unilaterally with 1.5x10^{6} IMR-32 cells with 30% matrigel (100µl total). Calipers were used to measure tumor diameter on two orthogonal

axes 2-3 times per week. Volume was calculated using the equation; $v = 4/3\pi r^3$ (where r = radius, calculated as an average of the two axes). Dosing occurred at predetermined mean tumor size of $0.24cm^3 \pm 0.09$ or $7mm \pm 0.09mm$ for 8 continuous days, *intravenous* with either indisulam 25 mg/kg or vehicle only (3.5% DMSO and 6.5% Tween 80 in saline) [6, 25]. Survival studies were terminated when the mean diameter of the tumor reached $1.9cm^3$, 14mm or after 66 days of tumor free disease, vehicle (n=6), indisulam (n=6). Pharmacodynamic study; mice were treated for four days. Tumour tissue were harvested (snap frozen or fixed in 4% paraformaldehyde) for further analysis, vehicle (n=5), indisulam (n=5).

In vivo model for neuroblastoma

Th-*MYCN* mice (129X1/SvJ-Tg(Th-*MYCN*)41Waw/Nci) have been described previously [26]. In this study, we used heterozygous Th-*MYCN* mice in which we observe 30% penetrance with tumor onset of 73 ± 25 days. Two to five mice were caged together and were allowed access to sterilized food and water *ad libitum*. Th-*MYCN* mice were monitored by palpation twice weekly and n=12 mice were enrolled into control group (n=6) or treated group (n=6) when tumors reached a palpation score of approximately 5 mm in diameter. Dosing was done for eight continuous days, *intravenous* with either indisulam 25 mg/kg or vehicle only (3.5% DMSO and 6.5% Tween 80 in saline). Studies were terminated when the tumor grew to a palpable size of 10 mm or immediately upon showing any signs of ill health. For survival analysis, mice were treated with indisulam were monitored for up to 124 days (n=5). Tumor size, animal weight, and overall animal well-being were scored daily throughout the study. One animal from the treated group was culled due to generalized ill-health at day 7; autopsy showed no macroscopic tumor residual but evidence of bowel obstruction.

MR images were acquired on a 1 Tesla M3 small animal MRI scanner (Aspect Imaging, Shoham, Israel). Mice were anaesthetised using isoflurane delivered via oxygen gas and their core temperature was maintained at 37C. Anatomical fat-suppressed T_2-weighted coronal images (TE=9ms, TR=4600ms) were acquired from 20 contiguous 1-mm-thick slices through the mouse abdomen, from which tumour volumes were determined using segmentation from regions of interest drawn on each tumour-containing slice using Horos medical image viewer. MRI was performed on a subgroup of mice throughout the study subject to equipment availability (n=4 vehicle, n=3 indisulam).

Protein analysis. Protein was extracted using RIPA buffer with 1% protease inhibitor (Sigma) and quantified using the BCA protein assay (ThermoScientific Pierce). 20µg of protein was loaded on a 4-20% Mini-Protean TGX pre-cast gel (Bio-Rad). Anti-RBM39 (HPA001591, Sigma) and Anti-beta-actin (ab8226, Abcam). CDK4 (ab108375, Abcam TYMS (ab108995, Abcam).

siRNA knockdown. IMR-32 or KELLY cells were seeded overnight in 96 or 6-well plates. Cells were transfected with SMARTpool DCAF15 siRNA (L-0.31237-01, Dharmacon, GE Healthcare) or a non-targeting control siRNA (NTC, D-001810-01-05) at a final concentration of 30nM and Lipofectamine 2000 transfection reagent (Invitrogen, UK). 6-well plates were treated with indisulam (vehicle control, 1µM or 10µM indisulam) 48hr post-transfection for 6hr and RNA/protein harvested accordingly. For RBM39 knockdown, HCT116 cells were transfected with SMARTpool RBM39 (L-011965-00, Dharmacon) or NTC at 30nM. Post-transfection RNA and protein was harvested for downstream analysis of mis-splicing and protein levels.

RNA extraction and PCR. Total RNA was extracted using the RNeasy Mini kit (Qiagen) according to the manufacturer's protocol. On-column DNase treatment was performed to remove contaminating genomic DNA. RNA concentration and purity was determined using the Nano-Drop Spectrometer (Nano-Drop Technologies, U.S.A). Reverse-transcription (RT) was performed on 2µg of RNA using the High-Capacity-RNA to cDNA kit (Applied Biosystems, U.K.) in a 20µL reaction. Exon skipping in *TRIM27* and *EZH2* was assessed using end-point PCR. 100ng cDNA was amplified with Q5® Hot Start High-Fidelity DNA Polymerase (New England BioLabs). Primers are noted in table 1.

Table 1. PCR primer sequences for end-point PCR

Gene	Forward and reverse sequences '5 to '3
TRIM27	CCTGAACCTTGGATCACACC GCAGGTCCTGTTGGAGGTAA
EZH2	CCGCTGAGGATGTGGATACT ACTCTCGGACAGCCAGGTAG
CDK4	GTGTATGGGGCCGTAGGAAC CCAACACTCCACATGTCCAC
GAPDH	GGCTGCTTTTAACTCTGG GGAGGGATCTCGCTCC

Immunofluorescence on tissue. Tumours were processed using a ASP300S tissue processor (Leica) according to the manufacturer's instructions. Sections were de-paraffinized and rehydrated through Histo-Clear and graded alcohol series, rinsed for 5 min in tap water, boiled for 5 min in 1% citric-acid buffer and left to cool to RT. Endogenous enzyme activity was blocked by 1% H_2O_2 for 20 min followed by 3 washes in ddH_2O. Sections were blocked for 1h in TBS 0.01% Triton (TBST), 5% BSA, RBM39 (HPA001591, Sigma, UK) or Ki67 (Cat #556003, BD Bioscience, UK) antibody was incubated at RT overnight 1:100, washed in TBST, 2nd Alexa Fluor 488/555 goat anti-rabbit antibody was incubated at RT for 1hr (1:500). Antibody solution; TBST, 5% BSA. Images were captured by confocal microscopy (LSM700, LSM T-PMT) and processed by ZEN2012 (Zeiss) software.

Metabolic analysis. The Seahorse Bioscience (Agilent Technologies) XFe96 analyser was used to measure extracellular acidification rate (ECAR) and oxygen consumption rate (OCR). Cells were seeded overnight at 60,000 cells/well. Wells were mixed for 3min and measurements were taken for 3min. The reported data points are the change in concentration over 3 minutes, recorded as mpH/minute for ECAR and pmol/minute for OCR. Protein content (BCA) was used for normalisation.

Fluorescence assays. The JC-1 mitochondrial membrane potential assay kit and the DCFDA/H_2DCFDA - Cellular Reactive Oxygen Species Detection assay kit were purchased from Abcam. For the JC-1 assay kit, 80,000 cells/well were seeded overnight. Cells were dosed with 10µM indisulam for 6hr and 5µM of reagent was used for the assay. For the DCFDA assay, 30,000 cells/well were seeded overnight. Cells were dosed with 100nM of indisulam for 72hr and the reagent was incubated with cells for 3hr and removed before fluorescence measurement. The manufacturer's guidelines were followed with appropriate positive controls and fluorescence was measured using the BMG LABTECH CLARIOstar plate reader. Biomass content (BCA or SRB) was used for normalisation.

GC-MS analysis. Samples were kept on dry ice throughout. Tumour samples were weighed and 20mg were used for analysis. Tissue was added to screw-cap tubes containing 0.1 mm glass beads (Bertin Technologies). 800µl of pre-chilled 80% methanol was added and samples were homogenised using a Precellys 24 bead beater (Bertin Technologies) set to 6500 rpm x 20 seconds x 2 cycles. Supernatants were collected after centrifugation (12,000g, 5min, at 4°C). The extraction was repeated and the fractions for each sample were pooled. Supernatants were then dried in a vacuum concentrator and subjected to dual-phase extraction. 300µl of chloroform/methanol (2:1) was added to each sample followed by

vortexing. 300µl of water was then added to each sample followed by vortexing and centrifugation (14,000rpm, 10 minutes at 4°C). The aqueous (upper) layer from each sample was transferred to silanized GC-MS vials. The dual-phase extraction was repeated and fractions were pooled for each sample.

In-house protocols adapted from previous reports [27] were used for GC-MS analysis, a summary is provided here. 10µl of 1.5 mg/ml myristic acid-d27 (internal standard) was added to each dried extract. Metabolites extracts were derivatised using the two-step method of derivatisation: methoxyamination and silylation [28]. When required, samples were diluted with anhydrous pyridine. Samples were analysed in a splitless mode on an Agilent 7890 GC with a 30 m DB-5MS capillary column and a 10m Duraguard column. This GC was coupled to an Agilent 5975 MSD [28]. Metabolites were assigned using FiehnLib assisted processing in AMDIS [29] and manually assessed using the Gavin package [27]

Metabolome analysis by LC-MS/MS. Cells were seeded to reach confluency in a 6-well plate format and then dosed with 10µM indisulam for 6hr. Parallel wells were counted for normalisation. A mixture of internal standards was added before extraction to account for variability during sample preparation. Cells were washed twice with 1 ml of Ringer's buffer and quenched with 1 ml of 80% cold methanol. After a 20min incubation on dry ice, cells were scraped, and the extract was transferred to 1.5 ml tubes. The wells were washed with another 0.5ml of 80% cold methanol and the extracts were pooled. Tubes were vortexed vigorously and spun down at 13,000rpm for 20min at 4°C. Supernatants were transferred to LC-MS vials and dried under nitrogen flow. Samples were stored at -40°C until LC-MS/MS analysis. Dry extracts were reconstituted at approximately 10,000 cells/µl with ACN/H2O (9:1) (positive and negative ionisation mode) or mobile phase B (negative ionisation mode).

Metabolites were separated at 50°C through an ACQUITY UPLC BEH amide column (1.7 µm, 2.1 x 150 mm) (Waters, MA, U.S.A.) using an in-house developed Hydrophilic Interaction Chromatography (HILIC) method. In negative mode, mobile phase was composed of A) 10mM ammonium hydroxide in acetonitrile and B) 20mM ammonium acetate, 10mM ammonium hydroxide in water. Chromatographic separation was achieved within 15min. The water composition was held at 10% for 1 min before ramping to 55% by 8 min, subsequently returning to 10% by 9.10 min for column re-equilibration. In positive mode, mobile phase was composed of A) 0.1% formic acid in acetonitrile and B) 0.1% formic acid, 20mM ammonium formate in water. The water composition was held at 5% for 1 min before ramping up to 50% by 8 min, subsequently returning to 5% by 9.10 min for column re-

equilibration. The flow rate was set to 0.5 ml/min and the total runtime was 45min per sample for both ionisation modes. The injection volume was set to 5µl and the samples were maintained at 8°C in the auto-sampler. For MS/MS analysis, an electrospray ionisation- triple quadrupole mass spectrometer (AB Sciex 4000) was used in the multiple reaction monitoring (MRM) mode. All methods were built using a scheduled MRM algorithm by applying a MRM detection window of 90 seconds and a target scan time of 2 seconds.

Protein identification and quantification by LC-MS/MS

Sample processing

Protein samples (50µg/replicate) were processed using the Filter Aided Sample Preparation (FASP) protocol [30]. Briefly, samples were loaded onto 30 kDa centrifugal concentrators (Millipore, MRCF0R030) and buffer exchange was carried out by centrifugation on a bench top centrifuge (15min, 12,000g). Multiple buffer exchanges were performed sequentially with UA buffer (8M urea in 100mM Tris pH 8.5, 3x200µl), reduction with 10mM DTT in UA buffer (30min, 40°C) and alkylation with 50mM chloroacetamide in UA buffer (20min, 25°C). This was followed by buffer exchange into UA buffer (3x100µl) and 50mM ammonium bicarbonate (3x100µl). Digestion was carried out with mass spectrometry grade trypsin (Promega, V5280) using 1µg protease per digest (16hr, 37°C). Tryptic peptides were collected by centrifugation into a fresh collection tube (10min, 12,000g) and washing of the concentrator with 0.5M sodium chloride (50µl, 10min, 12,000g) for maximal recovery. Following acidification with 1% trifluoroacetic acid (TFA) to a final concentration of 0.2%, collected protein digests were desalted using Glygen C18 spin tips (Glygen Corp, TT2C18.96) and peptides eluted with 60% acetonitrile, 0.1% formic acid (FA). Eluents were then dried using vacuum centrifugation.

Liquid chromatography-tandem mass spectrometry (LC-MS/MS) analysis

Dried tryptic digests were re-dissolved in 0.1% TFA by shaking (1200rpm) for 30min and sonication on an ultrasonic water bath for 10min, followed by centrifugation (20,000g, 5°C) for 10min. LC-MS/MS analysis was carried out in technical duplicates and separation was performed using an Ultimate 3000 RSLC nano liquid chromatography system (Thermo Scientific) coupled to a coupled to a Q-Exactive mass spectrometer (Thermo Scientific) via an EASY spray source (Thermo Scientific). For LC-MS/MS analysis protein digest solutions were injected and loaded onto a trap column (Acclaim PepMap 100 C18, 100µm × 2cm) for desalting and concentration at 8µl/min in 2% acetonitrile, 0.1% TFA. Peptides were then

eluted on-line to an analytical column (Acclaim Pepmap RSLC C18, 75µm × 75cm) at a flow rate of 200nl/min. Peptides were separated using a 120 minute gradient, 4-25% of buffer B for 90 minutes followed by 25-45% buffer B for another 30 minutes (composition of buffer B – 80% acetonitrile, 0.1% FA) and subsequent column conditioning and equilibration. Eluted peptides were analysed by the mass spectrometer operating in positive polarity using a data-dependent acquisition mode. Ions for fragmentation were determined from an initial MS1 survey scan at 70,000 resolution, followed by HCD (Higher Energy Collision Induced Dissociation) of the top 12 most abundant ions at 17,500 resolution. MS1 and MS2 scan AGC targets were set to 3e6 and 5e4 for maximum injection times of 50ms and 50ms respectively. A survey scan m/z range of 400 – 1800 was used, normalised collision energy set to 27%, charge exclusion enabled with unassigned and +1 charge states rejected and a minimal AGC target of 1e3.

Raw data processing

Data was processed using the MaxQuant software platform (v1.6.1.0), with database searches carried out by the in-built Andromeda search engine against the Uniprot *H.sapiens* database (version 20180104, number of entries: 161,521). A reverse decoy search approach was used at a 1% false discovery rate (FDR) for both peptide spectrum matches and protein groups. Search parameters included: maximum missed cleavages set to 2, fixed modification of cysteine carbamidomethylation and variable modifications of methionine oxidation, protein N-terminal acetylation and serine, threonine, tyrosine phosphorylation. Label-free quantification was enabled with an LFQ minimum ratio count of 2. 'Match between runs' function was used with match and alignment time limits of 1 and 20 minutes respectively.

Genomic analysis. Indisulam area under the curve (AUC) sensitivity data was acquired from The Cancer Target Discovery and Development (CTD2) Network [31]. Gene expression data was acquired from The Cancer Cell Line Encyclopaedia (CCLE) project, (https://portals.broadinstitute.org/ccle/home) and from The Cancer Therapeutics Response Portal http://portals.broadinstitute.org/ctrp) (Broad Institute).

Total RNA was extracted using the RNeasy Mini kit (Qiagen) and quantified by Qubit (Thermo Fisher) to assess sample integrity. Ribosomal and mitochondrial RNA were removed via ribodepletion. Seventy-five base paired end reads were sequenced by the Imperial BRC Genomics Facility using the HiSeq4000 (Illumina) resulting in ~45 million reads per sample. Data were aligned to the human reference genome (version hg19) using

HISAT2 (v 2.1.0) and BAM files were visualised using the Integrative Genome Viewer (Broad Institute). Read counts were quantified using function feature Counts from the R package Rsubread (v 1.34.7).

Proteomics analysis from IMR-32 cells subjected to 5μM indisulam for 6 and 16 hours was used for further analysis. The mean of three duplicates was taken and fold changes were calculated at 6hr and 16hr relative to the corresponding vehicle control. P-values were corrected using the Benjamini Hochberg method and were considered significant if <0.05. Further, genes that were identified as mis-spliced were compared with statistically significant up and down-regulated proteins (at 16hr indisulam exposure versus vehicle control). The overlap of which was then imported into the Consensus PathDB interaction database (provided by Max Planck Institute for Molecular Genetics http://cpdb.molgen.mpg.de/) for pathway enrichment analysis.

Alternative splicing analysis. SpliceFisher (github.com/jiwoongbio/SpliceFisher) was used to detect alternative splicing events, where exon and intron regions were defined from the hg19 human reference genome. To estimate differential exon skipping events, the number of exon-junction reads and exon skipping reads were calculated and compared with the vehicle control (Suppl. Fig. S1). Alternatively, for differential intron retention, the numbers of exon-intron and exon-exon reads were used. Read counts were evaluated by multiple Fisher's exact tests in three two-by-two tables using R, and p-values were adjusted using the Benjamini-Hochberg method and deemed significant p <0.05.

Data availability. The mass spectrometry proteomics data have been deposited to the ProteomeXchange Consortium via the PRIDE [32] partner repository with the dataset identifier PXD022164. The data discussed in this publication have been deposited in NCBI's Gene Expression Omnibus [33] and are accessible through GEO Series accession number 160446.

Results

Indisulam causes growth inhibition, selective depletion of RBM39 and global RNA mis-splicing in cellular models of neuroblastoma

We first sought to investigate tumour types that are likely to respond to aryl sulphonamides by probing publicly available databases with measurements of indisulam efficacy across 758

cancer cell lines [31]. When sensitivity (as Area under the Curve, AUC) was reviewed by tumour type, cell lines of the neuroblastoma lineage showed greatest sensitivity (Fig. 1a) in comparison with cell lines from other lineages (Mann-Whitney test, $p < 0.0001$; Fig. 1b). Indisulam efficacy was validated using a panel of *in vitro* models of neuroblastoma (IMR-32, LS, SHEP and KELLY). Indisulam induced growth inhibition and loss of viability in all four neuroblastoma cell lines (Fig. 1c-d) both in monolayer culture and in 3-D spheroids (Suppl. Fig. S2). An increased caspase activity was observed indicating cell death by apoptosis (Suppl. Fig. S2).

To confirm that indisulam induced selective RBM39 degradation in neuroblastoma, we performed LC-MS based global label-free proteomics following indisulam treatment in IMR-32 cells. After six hours treatment (5µM) we observed a highly selective loss of RBM39 abundance (~9 fold reduction) compared to ~4300 other detected proteins (Fig. 2a). The degradation of RBM39 was validated by western blot in two neuroblastoma cell lines; IMR-32 and KELLY (Fig. 2b) and the dependency on proteosome function for this response was confirmed by rescue with the proteasomal inhibitor bortezomib (Suppl. Figure S3). Since the loss of RBM39 is associated with defects in RNA splicing, we sought to identify transcripts that were affected following indisulam treatment in IMR-32 cells using total RNAseq. Stringent detection of altered events such as the skipping of cassette exons or the incorrect inclusion of introns was performed using *SpliceFisher* (github.com/jiwoongbio/SpliceFisher, [14]). Indisulam caused a high number of significant exon skipping (1893) and intron retention (1571) events (Fig. 2c). These include splicing events consistently reported subsequent to indisulam exposure such as the skipping of exon 6 and 7 of *TRIM27* (Fig. 2d – black arrows), and both exon skipping and intron retention in *EZH2* (Suppl. Fig. S4) [14, 15]. Using PCR assays we validated dose- and time-dependent exon skipping of *TRIM27* (Fig. 2e-f) and mis-splicing of *EZH2* (Suppl. Fig. S4) in both KELLY and IMR-32 cell lines. Collectively, these data were consistent with the hypothesis that selective degradation of RBM39 and defects in pre-mRNA splicing were likely to be the mechanism for the anti-proliferative effect of indisulam in neuroblastoma.

DCAF15 expression is necessary for the degradation of RBM39 and downstream mis-splicing

The expression of DCAF15 E3 ligase has been suggested to be critical for the mode of action of aryl sulphonamides including indisulam [14, 15]. To confirm that this was the case, we tested the correlation between gene expression and indisulam sensitivity using a large compound sensitivity data and gene expression for 758 cancer cell lines (The Cancer Target Discovery and Development Network [31]). Across all cell lines, sensitivity to indisulam was significantly correlated to *DCAF15* mRNA expression (Suppl. Fig. S5a). In addition, gene expression from over 1100 cell lines in the Cancer Cell Line Encyclopaedia (CCLE) database showed that levels of *DCAF15* in neuroblastoma cell lines was the highest among all solid tumour types (Suppl. Fig. S5b), further supporting the hypothesis that neuroblastoma patients could represent a target population for therapeutic intervention with aryl sulphonamides, such as indisulam.

To study the essentiality of DCAF15 in the mode of action of indisulam, we conducted knockdown experiments using siRNA interference in IMR-32 and KELLY cell lines. We show that indisulam sensitivity could be partially rescued in both KELLY and IMR-32 cells following DCAF15 knockdown (Fig. 3a). In addition, DCAF15 knockdown prevented RBM39 protein degradation (Fig. 3b), indicating that DCAF15 is necessary for this process. In accordance with this, mis-splicing in *TRIM27* (Fig. 3c) and *EZH2* (Suppl. Fig. S6) was not observed when DCAF15 was silenced. These findings support the hypotheses that the E3 ligase DCAF15 is necessary for indisulam-mediated growth inhibition and mis-splicing of pre-mRNA in neuroblastoma.

Indisulam abrogates proteins involved in cell cycle and metabolism through RBM39-mediated alternative splicing.

To capture the consequence of aberrant alternative splicing on protein levels in an unbiased way, we integrated transcriptomic and proteomic analyses post indisulam treatment in IMR-32 neuroblastoma cell line (5µM, 16hr). This multi-omic approach revealed that down-regulated proteins largely overlapped with transcripts that were mis-spliced (Fig. 4a-b) (231/367 (62%) of downregulated proteins were mis-spliced in contrast to 87/502 (17%) upregulated proteins). Of these 231 transcripts, the majority experienced intron retention (174/231 = 75%), which is in line with the observation that the presence of intron-retained transcripts correlates to reduced protein levels often through nonsense mediated decay (NMD) [34] To gain insight into the pathways affected by indisulam, the 231 target genes

were subjected to pathway enrichment analysis which revealed that pathways associated with cell cycle and metabolism were particularly affected. (Fig. 4b, full table in supplementary data). Indisulam was originally discovered as an inhibitor of cell cycle [3, 4] which is consistent with the enrichment among down-regulated proteins of those involved in cell cycle progression. By contrast, the observation that one-carbon and lipid pathways are affected by RBM39 loss has not been reported previously and could be more specific to neuroblastoma. To test the generalisability of these responses we compared highly significant observations in IMR-32 cells to responses in the colorectal cancer cell line HCT116, also known to be highly sensitive to indisulam [14, 35]. Proteomic analysis showed a significant decrease of the cyclin-dependent kinase CDK4 in both IMR-32 cells (logFC=-1.063, adj. p=3.73E-05; Fig. 4a) and in HCT116 (logFC=-0.473). Similarly, within the one-carbon pathway, thymidylate synthase (TYMS) was depleted in both IMR-32 (logFC=-1.169, adj.p=5.21E-05; Fig. 4a) and HCT116 cells (logFC=-1.212). Protein down-regulation of CDK4 and TYMS, as well as exon skipping of *CDK4* was independently validated in IMR-32 and KELLY cells (Fig. 4c-d).

To confirm that these events were specifically downstream of RBM39 loss, we conducted knockdown of RBM39 via siRNA in HCT116 cells and found mis-splicing of several genes, and a reduction of CDK4 and TYMS protein levels (Suppl. Fig. S7). Together, these data demonstrate that aberrant protein levels in cell cycle and metabolic pathways are a direct consequence of the loss of RBM39 and erroneous splicing of RNA following indisulam treatment and are not lineage specific responses to indisulam.

Indisulam perturbs redox balance and mitochondrial metabolism

Indisulam was previously reported to be a potent inhibitor of the extracellular carbonic anhydrase IX (CAIX) in cell-free assays [36]. Thus, indisulam might be expected to have a metabolic impact by preventing extracellular acidosis and consequently inhibiting glycolysis, however this mechanism has not previously been tested in cellular models of neuroblastoma. Extracellular acidification rate (ECAR), a proxy for glycolytic rate, and oxygen consumption rate (OCR) were therefore assessed in IMR-32 cells treated with indisulam. Notably, indisulam did not alter ECAR as anticipated but reduced OCR in cells determined by both the Seahorse Bioanalyzer (Fig. 5a-b) and MitoXpress assays (Suppl. Fig. S8). In addition, indisulam significantly increased levels of ROS (DCFDA fluorescence; Fig. 5c) and

depolarised the mitochondrial membrane (Δψm; Fig. 5d). These observations are however consistent with reported increases in mitochondrial superoxide and reduced OCR associated with RBM39 silencing in non-transformed hepatocytes [22]. Overall, these data indicate that indisulam affects mitochondrial metabolism in neuroblastoma cells and does not induce the metabolic phenotypes typically associated with CAIX inhibition.

To assess if indisulam affects metabolite levels on a wider scale, metabolomic changes were characterised using LC-MS/MS in IMR-32 neuroblastoma cell line. Acute treatment (6hr, 5μM) with indisulam induced significant increases in the pool sizes of many metabolites including non-essential amino acids (proline, serine, aspartate and glycine) and TCA-cycle intermediates (malate and fumarate) (Fig. 5e). Alterations in these pathways were validated using orthogonal GC-MS assays with significant metabolite changes confirmed in malate, serine, glycine and proline (Suppl. Fig. S9). Reactions such as the conversion of malate to aspartate are dependent on the reduction of NAD^+ to NADH while the conversion of proline to 1-pyrroline-5-carboxylate uses coenzyme FAD and reduces it to $FADH_2$ (Fig. 5f); thus an increased amount of these metabolites could also be linked to altered redox balance within the cells. To examine this, changes in the NADH/NAD^+ ratio in IMR-32 cells after indisulam treatment were investigated (Fig. 5g). This revealed a significant increase in the NADH/NAD^+ ratio in indisulam treated cells, confirming that redox balance is affected by treatment. In summary, these data show that indisulam causes significant impact on cellular metabolism including the accumulation of substrates for nucleotide synthesis and one carbon donors (aspartate, serine, glycine), consistent with the mis-splicing of biosynthetic genes in one-carbon metabolism. Furthermore, indisulam disrupted redox balance and mitochondrial oxidation, consistent with the known consequences of RBM39 depletion and ruling out CAIX inhibition as a likely mediator.

Indisulam is highly efficacious in two mouse models of neuroblastoma

Given that indisulam showed profound efficacy in a panel of neuroblastoma lines *in vitro*, indisulam was tested in an *in vivo* xenograft model. IMR-32 cells were subcutaneously injected into NCr Foxnnu mice, randomised and were dosed intravenously for eight days with indisulam (25mg/kg) or vehicle [6]. Complete tumour regression and a 100% survival rate (Fig. 6a-d) were reported in the treated group compared to the vehicle. Notably, no disease relapse was observed for up to 66 days after cessation of treatment. To study

pharmacodynamic markers and confirm mechanism of action *in vivo,* xenograft tissue was harvested after 4 days of treatment. This time point was chosen based on tumour sizes observed during survival study. At day 4, xenograft tumour volume was on average 94% of starting volume (indisulam arm n=5, 94% ± 48%, Suppl. Fig. S10). Immunofluorescence experiments revealed nuclear morphologic changes in indisulam treated mice, but cells remained positive for proliferation marker Ki67 (Suppl. Fig. S11). Xenograft tumours were analysed for RBM39 degradation (Fig. 6e) and mis-splicing of *CDK4* (Fig. 6f), demonstrating evidence of target engagement and mis-splicing of predicted genes confirming the downstream mode of action of indisulam *in vivo*. Xenograft tumours (4 days treatment) were also subjected to metabolic analysis via GC/MS (n=5 vehicle, n=5 indisulam; Suppl. Fig. S12) to validate metabolomic changes in the tumour. We observed a significant increase in amino acids proline, serine and glycine (Fig. 6g) in concordance with our *in vitro* observations in IMR-32 (Fig. 5e). Thus, we were able to demonstrate key pharmacodynamic (PD) responses to indisulam *in vivo* that provide proof-of-concept for target modulation and the proposed downstream mechanism of gene mis-splicing, protein depletion and altered metabolism in neuroblastoma models.

A second murine model was employed to establish further the efficacy of indisulam *in vivo*; a widely used Th-*MYCN* transgenic engineered mouse model (129X1/SvJ-Tg(Th-*MYCN*)41Waw/Nci). These tumours closely recapitulate many of the clinical and genomic features of high-risk neuroblastoma disease [26, 37]. We observed near complete reduction in tumour volume by MR imaging after 7 days of indisulam treatment compared to vehicle control (Fig. 7a-c). Importantly, no tumour relapse was reported over a period of more than 124 days (n=5) exemplifying the absence of recurrence (Fig. 7c). One animal in the treated group died at day 7, where the autopsy revealed no evidence of residual tumour but a bowel obstruction. Together these data indicate that indisulam may be a highly efficacious therapeutic agent for high-risk neuroblastoma.

Discussion

Until recently the key molecular event determining the anti-tumour activity of aryl sulphonamides, selective RBM39 degradation, was unknown and predictive biomarkers for therapy response unavailable. Since that discovery, a number of studies have detailed the structural basis of interactions between aryl sulphonamides, DCAF15 and RBM39, creating

both opportunities for the generation of novel protein degrading therapeutics based on DCAF15 targeting as well as new interest in RBM39 as an emerging anti-cancer target.

To the best of our knowledge, of the 47 clinical trials [Xu et al., 2020, in review] that have used indisulam or a related aryl sulphonamide, none have tested the efficacy of these compounds in patients with neuroblastoma. This is despite apparent evidence from public datasets demonstrating that neuroblastoma cell lines, together with a number of lymphoma and leukaemia models, exhibit high susceptibility to indisulam treatment (Figure 1, [31]). While recent studies in primary AML cells have confirmed this responsiveness [38] additional pre-clinical evidence for treatment of neuroblastoma was lacking.

Here, we have shown that aryl-sulphonamides are a viable and potent therapeutic strategy using multiple *in vivo* and *in vitro* neuroblastoma models including a transgenic mouse model of *MYCN*-driven, high-risk disease. Significantly, while indisulam has been assessed in a wide range of xenograft models including SW [25], LX-1, PC9, HCT15, HCT116 [6] and MML-AF9 leukemia cells [38], none modelled neuroblastoma and all previous experiments showed relapse after initial tumour regression once treatment was withdrawn. In contrast, we observe complete tumour response with prolonged remission after cessation of therapy, strongly underlining the fact that high-risk neuroblastoma may be particularly sensitive to indisulam.

Another novel aspect of our findings is the recognition that aryl sulphonamides may cause broad metabolic deficiencies and growth inhibition in cancer cells via the mechanism of RBM39 depletion and mis-splicing of specific genes which regulate metabolism and cell cycle. Although indisulam-induced depletion of RBM39 was previously reported to cause widespread RNA mis-splicing, these events are far from random. RBM39 knockdown coupled to CLIP-seq has indicated that RBM39 regulates a distinct set of splicing events from that of closely related spliceosomal factors U2AF65 and PUF60, enriched in cell cycle, RNA processing and metabolic pathway genes [21]. Specifically, we demonstrated that loss of RBM39 by either pharmacological or gene silencing is consistently associated with RNA splicing errors and reduced protein expression of critical factors for proliferation such as CDK4 and TYMS across different cell backgrounds. Targeted interference against CDK4/6 has been previously shown to cause G1 arrest in neuroblastoma [39], in part phenocopying indisulam. Indeed, we have recently shown that targeting cell cycle proteins (such as CDK2/9) are an increasingly important strategy for therapeutic developments in

neuroblastoma [40]. Likewise, silencing of RBM39 can reproduce several of the metabolic disruptions that we observe, such as a loss of oxidative metabolic capacity, altered redox balance and increases in serine and glycine, consistent with our findings [22]. As the serine/glycine/one-carbon metabolic pathway is closely linked to pyrimidine metabolism it is plausible that mis-splicing of TYMS activity could explain these observations, although CDK4 loss itself can reduce TYMS expression in a cell cycle independent manner [41]. Importantly, we confirm that these specific pharmacodynamic events translate to the *in vivo* setting, paving the way for their use as biomarkers for early evaluation of therapeutic response in clinic.

While we cannot rule out other RBM39-independent pathways contributing to indisulam-induced metabolic perturbations, such as the known inhibition of carbonic anhydrases by aryl sulphonamides in cell-free systems [36], the depletion of RBM39 appears to precede all other major molecular events and to be necessary for full efficacy. Overall, our data suggest that the loss of specific gene products downstream of RBM39 depletion, rather than global failure of the spliceosome, may best explain the toxicological sequelae of indisulam exposure and the variability in response in different tumours. With DCAF15 expression being an important determinant of sensitivity to indisulam [14, 15], high levels of DCAF15 in cells of neuroblastoma origin (Suppl. Fig. S3) might in part account for the high susceptibility of neuroblastoma to indisulam treatment observed in our current study. However, although our data support the hypothesis that DCAF15 expression is necessary for RBM39-depletion and anti-tumour activity of indisulam, a recent study suggested that DCAF15 levels in primary samples of tumour cells of AML patients did not correlate to RBM39 degradation [42], highlighting the need for additional predictive and pharmacodynamic biomarkers.

Amplification of the transcription factor N-Myc, which along with high c-Myc expression is frequently observed in high-risk neuroblastoma, leads to an increased oncogenic transcriptional program [43] whereby cells may rely more heavily on rapid and correct pre-mRNA processing and alternative splicing; thus the spliceosome has been described as the 'Achilles heel' of Myc-driven tumours [44]. For example it has been reported that N-Myc directly regulates an alternative splicing program by mediating splicing factor expression in high-risk neuroblastoma [45]. Protein degradation, whether through proteolysis targeting chimeras (PROTACS) or molecular glues like indisulam offer a new route to therapeutic targeting of spliceosomal components that may be difficult to drug due to lack of conventional active sites [46]. Interestingly, MYCN-amplified tumours are also more likely

to be sensitive to dual CDK4/6 inhibition [39] and plausibly therefore may also be more sensitive to CDK4 downregulation downstream of indisulam exposure and RBM39 depletion. Furthermore, N-Myc amplification reprogrammes metabolism in several ways including the serine-glycine synthesis and one-carbon metabolic pathway [47] and reactive oxygen species (ROS) production in neuroblastoma [48]. Combined, the increased dependency of neuroblastoma cells on metabolic reprogramming and RNA processing as a result of high N-Myc/c-Myc activity might be important factors that explain the sensitivity of high-risk neuroblastoma to indisulam.

Altogether, this study demonstrates high-risk neuroblastoma may be particularly sensitive to the dual targeting of metabolism and RNA splicing by the aryl sulphonamide indisulam. Since clinical PK data already exist and because treatment is well-tolerated in many patients, indisulam is a therapeutic that could be rapidly repurposed for clinical trials in high-risk neuroblastoma patients. Molecular profiling has revealed several specific gene and pathway level effects that could explain the high vulnerability of neuroblastoma to indisulam. The gene, protein and metabolite biomarkers identified in this study, in addition to DCAF15, provide a solid basis for confirming target engagement, monitoring early response to treatment and, in the future, for personalised therapy. Further studies on the essentiality of RBM39 and how cells may compensate for RBM39 loss could further optimise therapeutic targeting of RBM39 and accelerate biomarker-driven clinical trials.

554 **FIGURES**

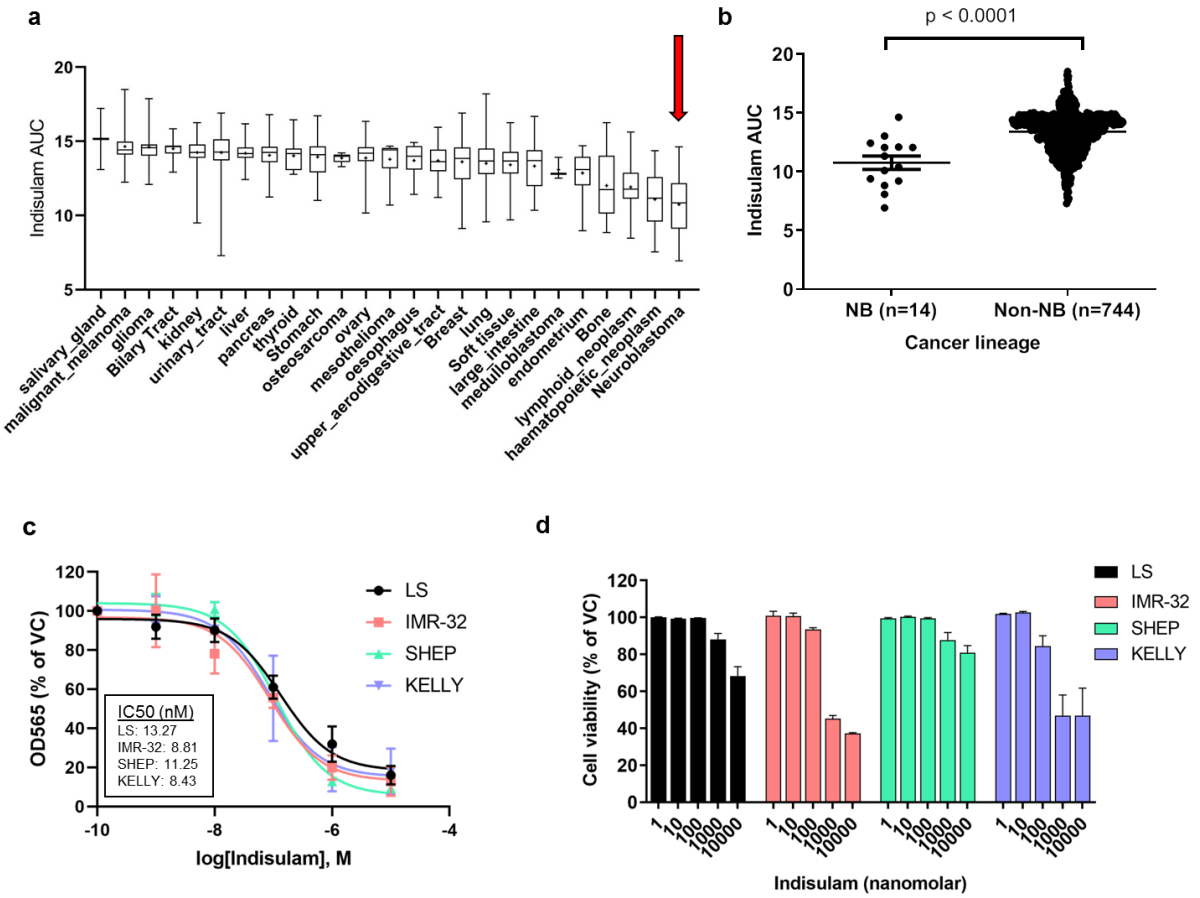

555 **Figure 1. Indisulam is efficacious in *in vitro* models of neuroblastoma. a** Indisulam area-
556 under-curve (AUC) in cell lines from 25 tumour origins. **b** Indisulam area-under-curve
557 (AUC) of 14 neural-crest derived neuroblastoma (NB) compared to non-NB cell lines (all
558 other cancer lineages). Each circle represents one cell line. Mann-Whitney test, p<0.0001.
559 Data was acquired from the CTD2 network [31]. **c** Cells were treated with a 5-point dose-
560 response of indisulam or vehicle control (0.1% DMSO) for 72hr. Cell growth determined
561 assessed by SRB assay (n=3, mean +/- SD). **d** Cells were treated with indisulam or vehicle
562 control (0.1% DMSO) for 72hr and cell viability was measured and normalised to the vehicle
563 control (n=2 for LS and IMR-32 and n=3 for SHEP, KELLY).

564

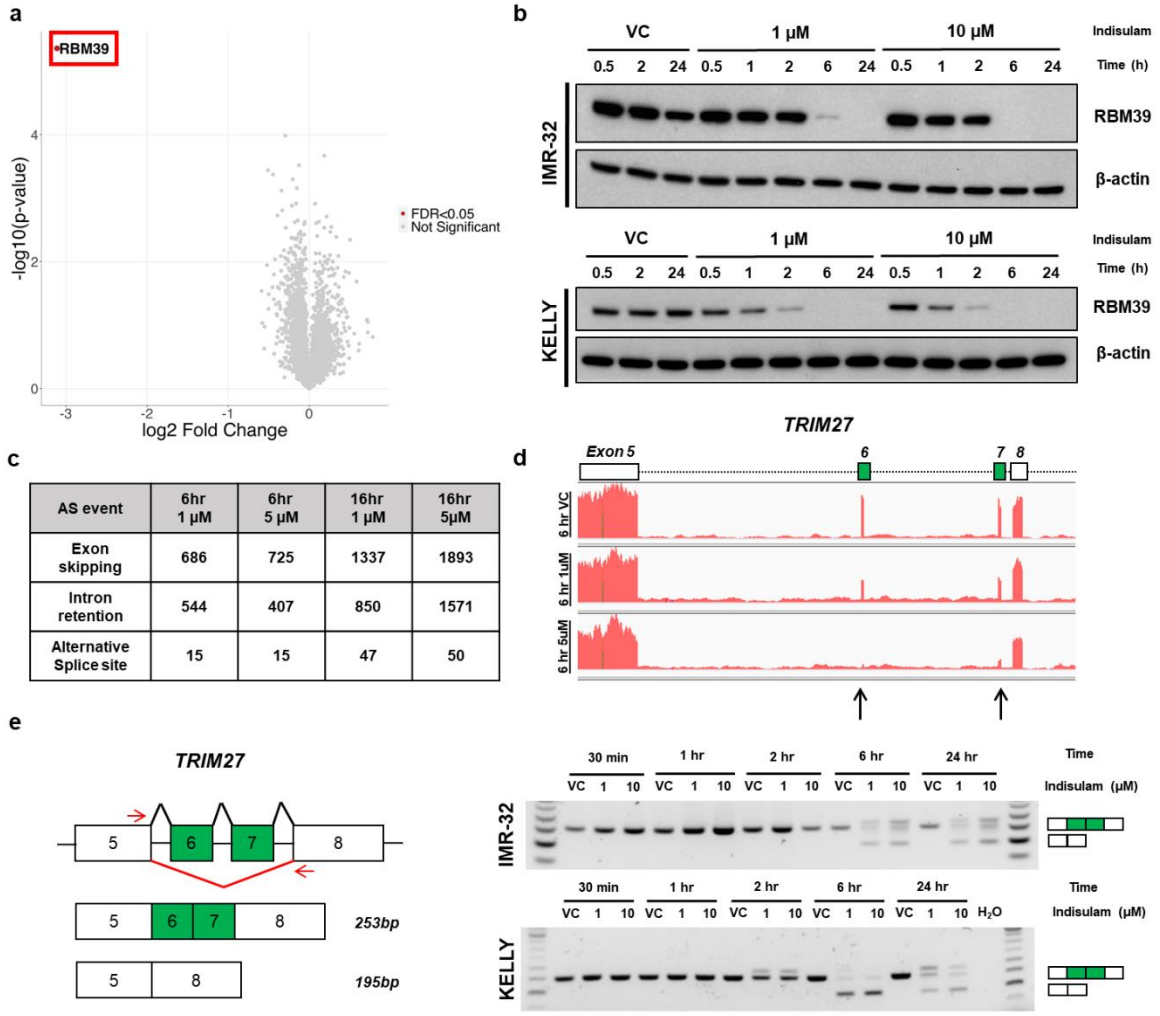

AS event	6hr 1 μM	6hr 5 μM	16hr 1 μM	16hr 5μM
Exon skipping	686	725	1337	1893
Intron retention	544	407	850	1571
Alternative Splice site	15	15	47	50

Figure 2. Indisulam causes selective degradation of RBM39 and subsequent mis-splicing. a Label-free proteomics of IMR-32 treated with 5μM indisulam or vehicle (VC, 0.1% DMSO). RBM39 selectively degraded 6hr post treatment. **b** KELLY and IMR-32 cells treated with VC, 1μM or 10μM indisulam for 0.5 to 24hr. Complete RBM39 degradation post 6hr of treatment in both cell lines. **c** RNAseq analysis of IMR-32 cells treated 5μM indisulam or VC (0.1% DMSO) for 6 or 16hr. Indisulam caused many exon skipping and intron retention events. **d** Read counts of *TRIM27* depict loss of exon 6 and 7 following indisulam (black arrows). **e** Indisulam causes skipping of exon 6 and 7 and skipping in both IMR-32 and KELLY cells, post RBM39 degradation.

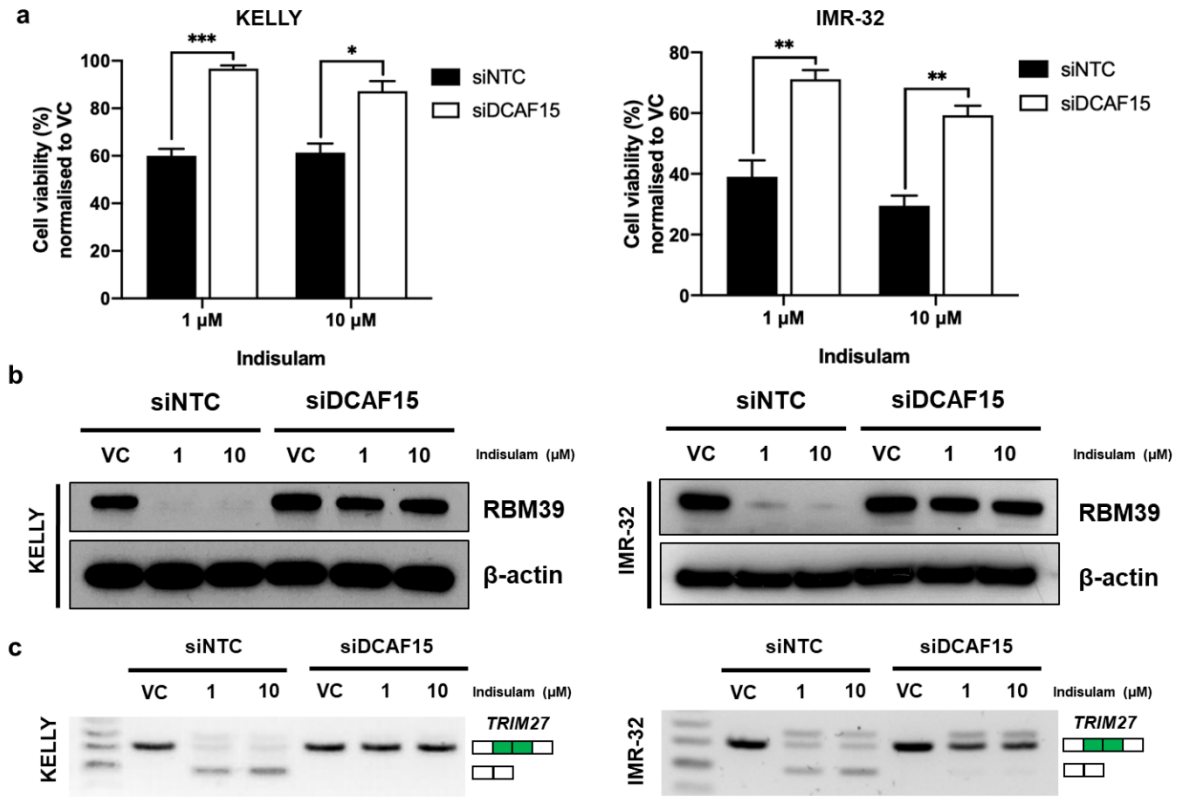

575 **Figure 3. Indisulam causes RBM39 degradation, loss of cell viability and mis-splicing in**
576 **a DCAF15-dependent manner. a** KELLY and IMR-32 cells transfected with control siRNA
577 (siNTC) or siRNA against DCAF15 (siDCAF15) and treated with vehicle or indisulam for
578 72hr and cell viability measured. **b** Western blot for RBM39 post-indisulam treatment in
579 KELLY and IMR-32 cells transfected with siNTC or siDCAF15. **c** *TRIM27* mis-splicing post
580 indisulam treatment in KELLY and IMR-32 cells transfected with siNTC or siDCAF15. Bars
581 represent mean +/- SD from three independent experiments. *p<0.05, **p<0.01 unpaired t-
582 test.

583

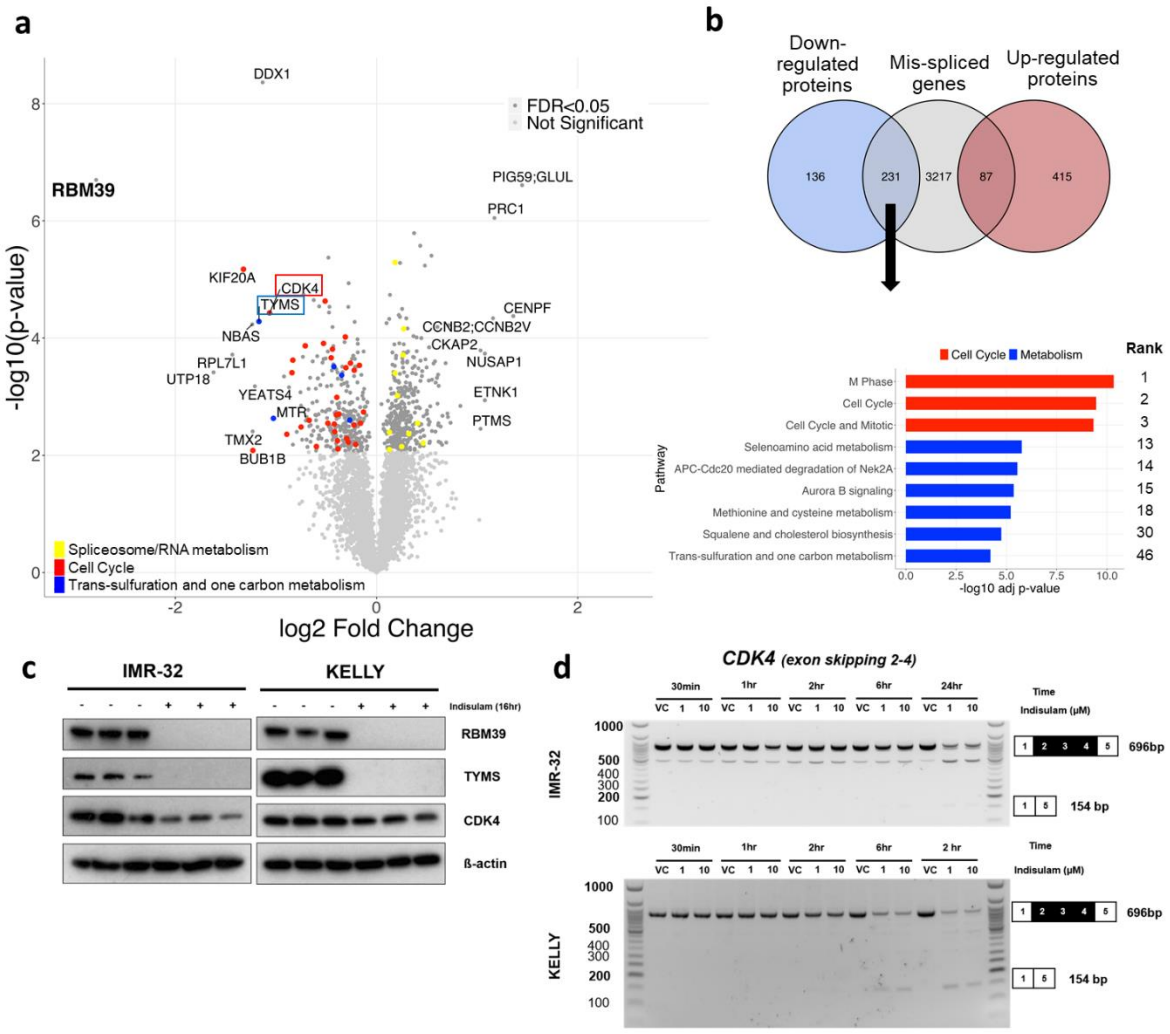

Figure 4. Indisulam-mediated RBM39 degradation leads to loss of proteins that regulate cell cycle and metabolism. a Label-free proteomics of IMR-32 treated with 5μM indisulam or VC (0.1% DMSO) for 16hr. **b** Overlap of splicing events (exon skipping and intron retention) with up or down-regulated proteins after 16hr of indisulam treatment. Gene ontology analysis of mis-spliced down-regulated proteins highlights cell cycle and various metabolic pathways. Full table in supplementary data. **c** Western blot confirming the reduction of TYMS and CDK4 in IMR-32 and KELLY treated with indisulam or vehicle for 16hr. **d** Indisulam causes time and dose-dependent skipping of exon 2 to 4 of *CDK4* in both IMR-32 and KELLY cells, post RBM39 degradation.

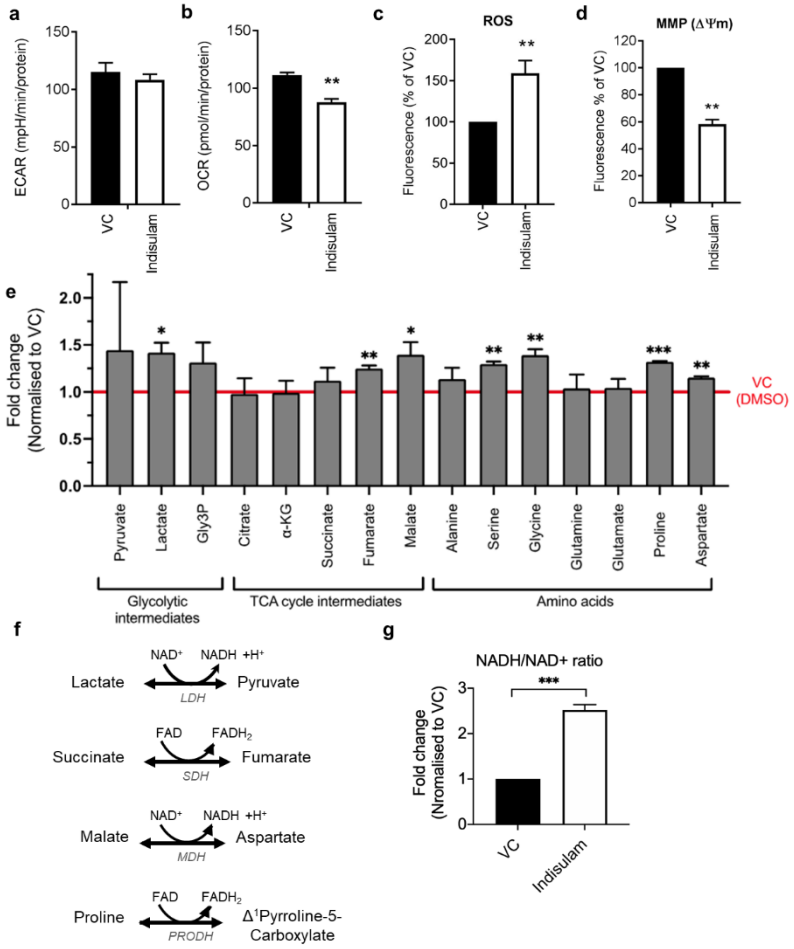

Figure 5. Indisulam disrupts cellular metabolism. a Extracellular acidification rate (ECAR) and **b** oxygen consumption rate (OCR) of IMR-32 cells after 1hr of treatment with 10µM indisulam. **p<0.01 unpaired t-test. **c** ROS levels of IMR-32 cells after 72hr of treatment with 100nM indisulam. ROS production was measured by DCFDA fluorescence emission at 535 nm. % of vehicle control fluorescence is shown. **p<0.01 one-sample t-test. **d** The mitochondrial membrane potential (MMP) of IMR-32 cells after 6hr of treatment with 10µM indisulam. MMP was measured by JC-1 aggregate fluorescence emission at 590 nm. % of vehicle control fluorescence is shown. **p>0.01 one-sample t-test. **e** LC-MS/MS profiling of IMR-32 cells after 6hr of treatment with indisulam (10µM). Data are normalised to vehicle control (VC, 0.1% DMSO) which is marked by a red line. *p < 0.05, **p < 0.01, ***p < 0.001 unpaired t-test. **f** Schematic of enzymatic reactions involving the conversion of NAD+ to NADH or FAD to FADH. **g** Ratio of NADH/NAD+ after 6hr treatment with indisulam (10µM) or vehicle control. ***p<0.001, unpaired t-test**.** All vehicle controls are 0.1% DMSO. All bars represent mean +/- SD.

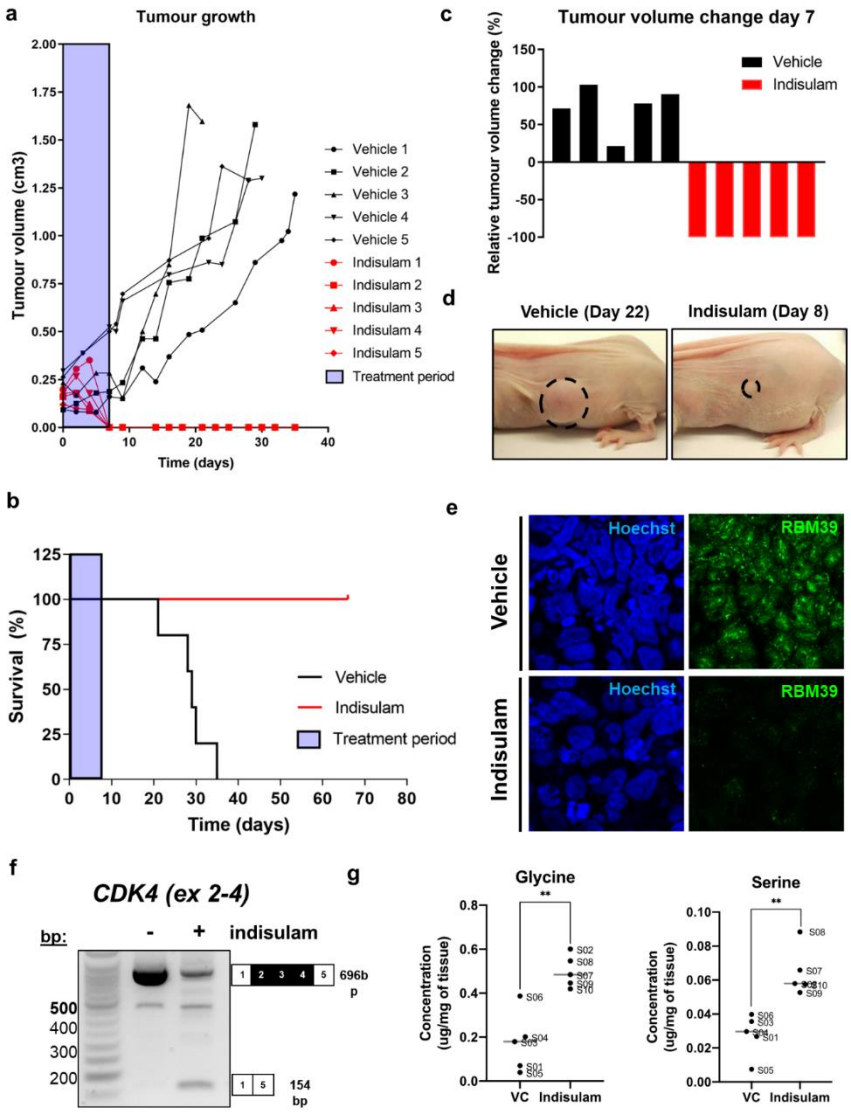

611

612 **Figure 6. Indisulam is efficacious and causes RBM39 depletion, RNA mis-splicing and**
613 **metabolic perturbations in neuroblastoma *in vivo*.** **a** Tumour growth in mice bearing IMR-
614 32 xenografts treated with either vehicle (n=5) or indisulam (n=5) for eight days. Tumour
615 volume measured every 2-3 days. **b** Survival plot of mice bearing IMR-32 xenografts. **c**
616 Waterfall plot showing relative changes in tumour volume of xenografts at day 7. **d**
617 Representative images of IMR-32 xenografts treated with vehicle (day 22) or indisulam (day
618 8). **e-g** IMR-32 xenografts bearing mice were treated with vehicle or indisulam for 4 days to
619 assess pharmacodynamic markers and metabolism in tumours. **e** RBM39 degradation
620 determined by immunofluorescence on fixed tissues. **f** Exon skipping of *CDK4* in RNA
621 extracted from IMR-32 xenograft tumours**. g** Glycine and serine changes detected by GC-MS
622 of xenograft tumour tissues (n=5 per group). **p<0.01, unpaired t-test.

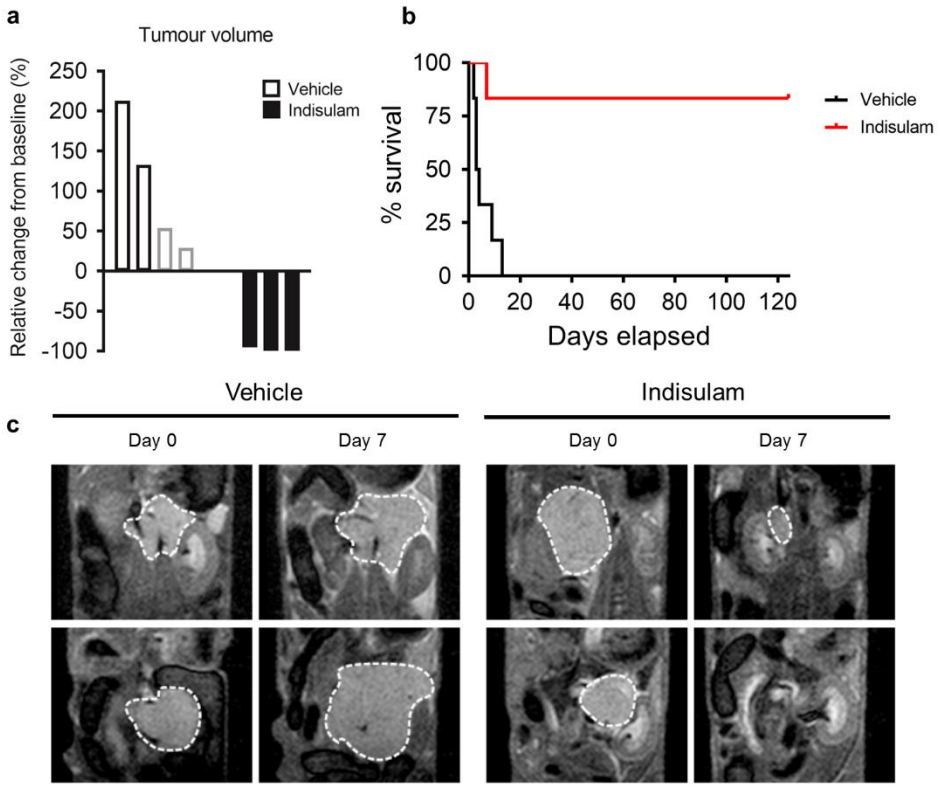

623 **Figure 7. Indisulam is efficacious in a Th-*MYCN* transgenic mouse of neuroblastoma.**
624 **a** Waterfall plot showing the relative changes in tumour volume in the Th-*MYCN* transgenic
625 mice treated for seven days with indisulam (n=3) or vehicle control (n=4) measured by MRI.
626 Note that the mice represented by the grey bars reached the tumour size study endpoint
627 (palpation) before their Day 7 MRI scan and the data shown for these two mice are the
628 relative changes in volume following at day 3 of treatment with indisulam. **b** Survival of mice
629 treated with vehicle (n=6) or indisulam (n=6). One mouse in indisulam treated group died on
630 day 7. Autopsy revealed no presence of tumour but evidence of bowel obstruction.
631 **c** Representative anatomical coronal T_2-weighted MRI of the abdomen of Th-*MYCN* mice
632 prior (day 0) and following seven days of treatment with indisulam or vehicle control.
633 Dashed white line indicates the tumour circumference.

634

635 **REFERENCES**

636 1. London, W.B., et al., *Clinical and biologic features predictive of survival after*
637 *relapse of neuroblastoma: a report from the International Neuroblastoma Risk Group*
638 *project.* J Clin Oncol, 2011. **29**(24): p. 3286-92.
639 2. Colon, N.C. and D.H. Chung, *Neuroblastoma.* Adv Pediatr, 2011. **58**(1): p. 297-311.
640 3. Owa, T., et al., *Discovery of novel antitumor sulfonamides targeting G1 phase of the*
641 *cell cycle.* J Med Chem, 1999. **42**(19): p. 3789-99.
642 4. Yoshino, H., et al., *Novel sulfonamides as potential, systemically active antitumor*
643 *agents.* J Med Chem, 1992. **35**(13): p. 2496-7.
644 5. Fukuoka, K., et al., *Mechanisms of action of the novel sulfonamide anticancer agent*
645 *E7070 on cell cycle progression in human non-small cell lung cancer cells.* Invest
646 New Drugs, 2001. **19**(3): p. 219-27.
647 6. Ozawa, Y., et al., *E7070, a novel sulphonamide agent with potent antitumour activity*
648 *in vitro and in vivo.* Eur J Cancer, 2001. **37**(17): p. 2275-82.
649 7. Raymond, E., et al., *Phase I and pharmacokinetic study of E7070, a novel*
650 *chloroindolyl sulfonamide cell-cycle inhibitor, administered as a one-hour infusion*
651 *every three weeks in patients with advanced cancer.* J Clin Oncol, 2002. **20**(16): p.
652 3508-21.
653 8. Terret, C., et al., *Phase I clinical and pharmacokinetic study of E7070, a novel*
654 *sulfonamide given as a 5-day continuous infusion repeated every 3 weeks in patients*
655 *with solid tumours. A study by the EORTC Early Clinical Study Group (ECSG).* Eur J
656 Cancer, 2003. **39**(8): p. 1097-104.
657 9. Dittrich, C., et al., *Phase I and pharmacokinetic study of E7070, a chloroindolyl-*
658 *sulfonamide anticancer agent, administered on a weekly schedule to patients with*
659 *solid tumors.* Clin Cancer Res, 2003. **9**(14): p. 5195-204.
660 10. Haddad, R.I., et al., *A phase II clinical and pharmacodynamic study of E7070 in*
661 *patients with metastatic, recurrent, or refractory squamous cell carcinoma of the*
662 *head and neck: modulation of retinoblastoma protein phosphorylation by a novel*
663 *chloroindolyl sulfonamide cell cycle inhibitor.* Clin Cancer Res, 2004. **10**(14): p.
664 4680-7.
665 11. Punt, C.J., et al., *Phase I and pharmacokinetic study of E7070, a novel sulfonamide,*
666 *given at a daily times five schedule in patients with solid tumors. A study by the*
667 *EORTC-early clinical studies group (ECSG).* Ann Oncol, 2001. **12**(9): p. 1289-93.
668 12. Talbot, D.C., et al., *A randomized phase II pharmacokinetic and pharmacodynamic*
669 *study of indisulam as second-line therapy in patients with advanced non-small cell*
670 *lung cancer.* Clin Cancer Res, 2007. **13**(6): p. 1816-22.
671 13. Yamada, Y., et al., *Phase I pharmacokinetic and pharmacogenomic study of E7070*
672 *administered once every 21 days.* Cancer Sci, 2005. **96**(10): p. 721-8.
673 14. Han, T., et al., *Anticancer sulfonamides target splicing by inducing RBM39*
674 *degradation via recruitment to DCAF15.* Science, 2017. **356**(6336).
675 15. Uehara, T., et al., *Selective degradation of splicing factor CAPERalpha by anticancer*
676 *sulfonamides.* Nat Chem Biol, 2017. **13**(6): p. 675-680.
677 16. Dowhan, D.H., et al., *Steroid hormone receptor coactivation and alternative RNA*
678 *splicing by U2AF65-related proteins CAPERalpha and CAPERbeta.* Mol Cell, 2005.
679 **17**(3): p. 429-39.
680 17. Stepanyuk, G.A., et al., *UHM-ULM interactions in the RBM39-U2AF65 splicing-*
681 *factor complex.* Acta Crystallogr D Struct Biol, 2016. **72**(Pt 4): p. 497-511.

18. Loerch, S., et al., *Cancer-relevant splicing factor CAPERalpha engages the essential splicing factor SF3b155 in a specific ternary complex.* J Biol Chem, 2014. **289**(25): p. 17325-37.
19. Dutta, J., G. Fan, and C. Gelinas, *CAPERalpha is a novel Rel-TAD-interacting factor that inhibits lymphocyte transformation by the potent Rel/NF-kappaB oncoprotein v-Rel.* J Virol, 2008. **82**(21): p. 10792-802.
20. Jung, D.J., et al., *Molecular cloning and characterization of CAPER, a novel coactivator of activating protein-1 and estrogen receptors.* J Biol Chem, 2002. **277**(2): p. 1229-34.
21. Mai, S., et al., *Global regulation of alternative RNA splicing by the SR-rich protein RBM39.* Biochim Biophys Acta, 2016. **1859**(8): p. 1014-24.
22. Kang, Y.K., et al., *CAPER is vital for energy and redox homeostasis by integrating glucose-induced mitochondrial functions via ERR-alpha-Gabpa and stress-induced adaptive responses via NF-kappaB-cMYC.* PLoS Genet, 2015. **11**(4): p. e1005116.
23. Workman, P., et al., *Guidelines for the welfare and use of animals in cancer research.* Br J Cancer, 2010. **102**(11): p. 1555-77.
24. Kilkenny, C., et al., *Improving bioscience research reporting: the ARRIVE guidelines for reporting animal research.* Vet Clin Pathol, 2012. **41**(1): p. 27-31.
25. Ozawa, Y., et al., *Therapeutic potential and molecular mechanism of a novel sulfonamide anticancer drug, indisulam (E7070) in combination with CPT-11 for cancer treatment.* Cancer Chemother Pharmacol, 2012. **69**(5): p. 1353-62.
26. Weiss, W.A., et al., *Targeted expression of MYCN causes neuroblastoma in transgenic mice.* EMBO J, 1997. **16**(11): p. 2985-95.
27. Behrends, V., G.D. Tredwell, and J.G. Bundy, *A software complement to AMDIS for processing GC-MS metabolomic data.* Anal Biochem, 2011. **415**(2): p. 206-8.
28. Kind, T., et al., *FiehnLib: mass spectral and retention index libraries for metabolomics based on quadrupole and time-of-flight gas chromatography/mass spectrometry.* Anal Chem, 2009. **81**(24): p. 10038-48.
29. Stein, S.E., *An integrated method for spectrum extraction and compound identification from gas chromatography/mass spectrometry data.* Journal of the American Society for Mass Spectrometry, 1999. **10**(8): p. 770-781.
30. Wisniewski, J.R., et al., *Universal sample preparation method for proteome analysis.* Nat Methods, 2009. **6**(5): p. 359-62.
31. Rees, M.G., et al., *Correlating chemical sensitivity and basal gene expression reveals mechanism of action.* Nat Chem Biol, 2016. **12**(2): p. 109-16.
32. Perez-Riverol, Y., et al., *The PRIDE database and related tools and resources in 2019: improving support for quantification data.* Nucleic Acids Res, 2019. **47**(D1): p. D442-D450.
33. Edgar, R., M. Domrachev, and A.E. Lash, *Gene Expression Omnibus: NCBI gene expression and hybridization array data repository.* Nucleic Acids Res, 2002. **30**(1): p. 207-10.
34. Braunschweig, U., et al., *Widespread intron retention in mammals functionally tunes transcriptomes.* Genome Res, 2014. **24**(11): p. 1774-86.
35. Bussiere, D.E., et al., *Structural basis of indisulam-mediated RBM39 recruitment to DCAF15 E3 ligase complex.* Nat Chem Biol, 2020. **16**(1): p. 15-23.
36. Abbate, F., et al., *Carbonic anhydrase inhibitors: E7070, a sulfonamide anticancer agent, potently inhibits cytosolic isozymes I and II, and transmembrane, tumor-associated isozyme IX.* Bioorg Med Chem Lett, 2004. **14**(1): p. 217-23.

37. Chesler, L. and W.A. Weiss, *Genetically engineered murine models--contribution to our understanding of the genetics, molecular pathology and therapeutic targeting of neuroblastoma.* Semin Cancer Biol, 2011. **21**(4): p. 245-55.
38. Wang, E., et al., *Targeting an RNA-Binding Protein Network in Acute Myeloid Leukemia.* Cancer Cell, 2019. **35**(3): p. 369-384 e7.
39. Rader, J., et al., *Dual CDK4/CDK6 inhibition induces cell-cycle arrest and senescence in neuroblastoma.* Clin Cancer Res, 2013. **19**(22): p. 6173-82.
40. Poon, E., et al., *Orally bioavailable CDK9/2 inhibitor shows mechanism-based therapeutic potential in MYCN-driven neuroblastoma.* J Clin Invest, 2020.
41. Le Francois, B.G., J.A. Maroun, and H.C. Birnboim, *Expression of thymidylate synthase in human cells is an early G(1) event regulated by CDK4 and p16INK4A but not E2F.* Br J Cancer, 2007. **97**(9): p. 1242-50.
42. Hsiehchen, D., et al., *Biomarkers for RBM39 degradation in acute myeloid leukemia.* Leukemia, 2020.
43. Burgess, D.J., *MYC provides a global boost.* Nature Reviews Genetics, 2012. **13**(11): p. 758-758.
44. Anczukow, O. and A.R. Krainer, *The spliceosome, a potential Achilles heel of MYC-driven tumors.* Genome Med, 2015. **7**: p. 107.
45. Zhang, S., et al., *MYCN controls an alternative RNA splicing program in high-risk metastatic neuroblastoma.* Cancer Lett, 2016. **371**(2): p. 214-24.
46. Toure, M. and C.M. Crews, *Small-Molecule PROTACS: New Approaches to Protein Degradation.* Angew Chem Int Ed Engl, 2016. **55**(6): p. 1966-73.
47. Xia, Y., et al., *Metabolic Reprogramming by MYCN Confers Dependence on the Serine-Glycine-One-Carbon Biosynthetic Pathway.* Cancer Res, 2019. **79**(15): p. 3837-3850.
48. Wang, T., et al., *MYCN drives glutaminolysis in neuroblastoma and confers sensitivity to an ROS augmenting agent.* Cell Death Dis, 2018. **9**(2): p. 220.

Acknowledgements

This work was funded by the Imperial College Medical Research Council (MRC) Doctoral Training Programme (DTP), grant number: MR/K501281 and by MetaCELL-TM H2020 Fast Track to Innovation (737978). Infrastructure for this research was supported by the Imperial Experimental Cancer Medicine Centre and the Cancer Research UK Imperial Centre as well as the National Institute for Health Research (NIHR) Imperial Biomedical Research Centre (including the Imperial Genomics Facility). Cancer Research UK also support the Cancer Imaging Centre at ICR, in association with the MRC and Department of Health (England) (C1060/A16464). O.Y., E.P., B.M.C., and L.C. are funded by Cancer Research UK (C34648/A18339 and C34648/A28278). Y.J. is a Children with Cancer UK Research Fellow (2014/176). A.N. is funded through an AstraZeneca/Imperial College Research Fellowship (2019).

Author contributions

A.N., A.S., O.Y., Y.J., L.C., and H.C.K., conceived the study, designed the experiments and interpreted data. A.N., A.S., L.H., E.P., Y.L., acquired data from cellular experiments with the guidance of A.B. and E.W. on methodology. O.Y., Y.J. and B.M.C. performed and acquired data from *in vivo* experiments, including imaging. H.K. and A.M. performed proteomics and processing of data with the guidance of D.C. on methodology. A.S. L.H. and E. K. performed mass spectrometry of *in vitro* and *in vivo* samples, processed and analysed data. C.E. and G.V. analysed RNAseq and proteomics data. All authors contributed to the writing and editing of the manuscript.

Competing interests

All authors declare no competing interests

Supplementary.

p-value	q-value	pathway	source
7.38E-12	3.34E-09	M Phase	Reactome
8.48E-10	1.55E-07	Cell Cycle	Reactome
1.02E-09	1.55E-07	Cell Cycle, Mitotic	Reactome
9.47E-09	9.63E-07	Mitotic Prometaphase	Reactome
1.06E-08	9.63E-07	Separation of Sister Chromatids	Reactome
2.68E-08	1.65E-06	Mitotic Anaphase	Reactome
2.78E-08	1.65E-06	Mitotic Spindle Checkpoint	Reactome
2.91E-08	1.65E-06	Mitotic Metaphase and Anaphase	Reactome
9.04E-08	4.55E-06	ensation of Prometaphase Chromos	Reactome
2.07E-07	9.38E-06	Aurora B signaling	PID
8.91E-07	3.67E-05	pr-mediated nuclear import of PIC	Reactome
9.77E-07	3.69E-05	Aminosugars metabolism	EHMN
1.55E-06	5.08E-05	actions of Vpr with host cellular pro	Reactome
1.57E-06	5.08E-05	Methionine and cysteine metabolism	EHMN
1.85E-06	5.21E-05	Selenoamino acid metabolism	EHMN
2.15E-06	5.21E-05	APC/C via direct inhibition of the A	Reactome
2.15E-06	5.21E-05	required for the onset of anaphas	Reactome
2.16E-06	5.21E-05	solution of Sister Chromatid Cohes	Reactome
2.23E-06	5.21E-05	Cell Cycle Checkpoints	Reactome
2.30E-06	5.21E-05	dependent Golgi-to-ER retrograde	Reactome
6.67E-06	0.00014384	Cdc20 mediated degradation of Ne	Reactome
7.57E-06	0.00014902	om unattached kinetochores via a	Reactome
7.57E-06	0.00014902	ification of signal from the kinetoc	Reactome
9.80E-06	0.00018488	spho-APC/C mediated degradation	Reactome
1.17E-05	0.00021266	of cell cycle proteins prior to satis	Reactome
1.28E-05	0.00021814	tRNA processing	Reactome
1.40E-05	0.00021814	of Ribonucleoproteins into the Ho	Reactome
1.40E-05	0.00021814	Glucokinase by Glucokinase Regul	Reactome
1.40E-05	0.00021814	Interacts with the Cellular Export N	Reactome
1.65E-05	0.00024125	20 mediated degradation of mitot	Reactome
1.65E-05	0.00024125	of Viral Ribonucleoproteins from N	Reactome
1.94E-05	0.00027437	d APC/C:Cdc20 mediated degradat	Reactome
2.00E-05	0.00027437	Mitotic Prophase	Reactome
2.27E-05	0.00029347	rt of the SLBP independent Matur	Reactome
2.27E-05	0.00029347	-mediated nuclear export of HIV R	Reactome
2.64E-05	0.00031423	Nuclear import of Rev protein	Reactome
2.64E-05	0.00031423	ort of the SLBP Dependant Mature	Reactome
2.64E-05	0.00031423	lear Pore Complex (NPC) Disassem	Reactome
2.87E-05	0.00033375	tRNA processing in the nucleus	Reactome
2.98E-05	0.00033571	ellular responses to external stimu	Reactome
3.04E-05	0.00033571	Golgi-to-ER retrograde transport	Reactome
3.51E-05	0.00037872	PC/C activators between G1/S and	Reactome

4.03E-05	0.00040527	qualene and cholesterol biosynthes	EHMN
4.03E-05	0.00040527	MOylation of DNA replication prote	Reactome
4.03E-05	0.00040527	actions of Rev with host cellular pr	Reactome
4.63E-05	0.00045602	RHO GTPases Activate Formins	Reactome
5.54E-05	0.00053353	phatidylinositol phosphate metabo	EHMN
5.92E-05	0.00055917	ature mRNA Derived from an Intro	Reactome
6.69E-05	0.00059433	nediated degradation of cell cycle	Reactome
6.69E-05	0.00059433	Regulation of mitotic cell cycle	Reactome
6.69E-05	0.00059433	lature mRNAs Derived from Intronl	Reactome
6.97E-05	0.00060691	Cellular responses to stress	Reactome
7.53E-05	0.00064373	Viral Messenger RNA Synthesis	Reactome
8.56E-05	0.000718	Glycosphingolipid metabolism	EHMN
9.28E-05	0.00076442	Glycolysis	Reactome
9.45E-05	0.00076476	za Viral RNA Transcription and Rep	Reactome
0.00011038	0.0008772	h O-[N-acetyl]-glucos	HumanCyc
0.00011733	0.00090086	Fanconi anemia pathway	PID
0.00011733	0.00090086	UMOylation of RNA binding protein	Reactome
0.00012599	0.00093566	erpathway of cholesterol biosynth	HumanCyc
0.00012599	0.00093566	Cholesterol biosynthesis	Reactome
0.00013167	0.00096206	Membrane Trafficking	Reactome
0.00013722	0.00098664	Metabolism of RNA	Reactome
0.00016971	0.00119845	serine, alanine and threonine met	EHMN
0.00017196	0.00119845	amin D3 (cholecalciferol) metaboli	EHMN
0.00019276	0.00132306	Nuclear Envelope Breakdown	Reactome
0.00021148	0.00140883	snRNP Assembly	Reactome
0.00021148	0.00140883	Metabolism of non-coding RNA	Reactome
0.00022895	0.00149845	Pentose phosphate pathway	EHMN
0.00023155	0.00149845	Influenza Life Cycle	Reactome
0.00025304	0.00161444	anemia pathway - Homo sapiens (	KEGG
0.00027862	0.00175298	Vesicle-mediated transport	Reactome
0.0002984	0.00180234	-sulfuration and one carbon metab	Wikipathways
0.0002984	0.00180234	B5 - CoA biosynthesis from pantot	EHMN
0.0002984	0.00180234	din formation from dihomo gama-l	EHMN
0.00033201	0.00197898	RHO GTPase Effectors	Reactome
0.00034931	0.00205504	Host Interactions of HIV factors	Reactome
0.00037106	0.00215501	Glucose metabolism	Reactome
0.0003834	0.00219847	role in mitosis and chromosome dy	BioCarta
0.00047556	0.00269284	Cholesterol Biosynthesis Pathway	Wikipathways
0.00052135	0.00291568	Influenza Infection	Reactome
0.00061816	0.00341494	Cellular response to heat stress	Reactome
0.00064636	0.00352774	Glycolysis and Gluconeogenesis	EHMN
0.00074136	0.00399804	tory Element-Binding Proteins (SRE	Wikipathways
0.00078801	0.00419964	-Golgi and retrograde Golgi-to-ER t	Reactome
0.00084642	0.00445847	ylation of chromatin organization p	Reactome

0.00097049	0.00505325	-Inflammatory metabolites formati	EHMN
0.00102432	0.00514183	e mRNA derived from an Intron-Co	Reactome
0.00106136	0.00514183	De novo fatty acid biosynthesis	EHMN
0.00106136	0.00514183	Vitamin E metabolism	EHMN
0.00114641	0.00514183	Phosphorylation of the APC/C	Reactome
0.00114641	0.00514183	om APC/C:Cdc20 to APC/C:Cdh1 in	Reactome
0.00114641	0.00514183	tion of gene expression by SREBF (S	Wikipathways
0.00114641	0.00514183	ylhomocysteine (SAH) Hydrolase D	SMPDB
0.00114641	0.00514183	Methionine Metabolism	SMPDB
0.00114641	0.00514183	hionine Adenosyltransferase Defici	SMPDB
0.00114641	0.00514183	ycine N-methyltransferase Deficien	SMPDB
0.00114641	0.00514183	Hypermethioninemia	SMPDB
0.00114641	0.00514183	trahydrofolate Reductase Deficien	SMPDB
0.00114641	0.00514183	ia due to defect in cobalamin meta	SMPDB
0.00114641	0.00514183	stathionine Beta-Synthase Deficien	SMPDB
0.00121927	0.00535519	HIV Life Cycle	Reactome
0.00122858	0.00535519	n of DNA damage response and rep	Reactome
0.00148493	0.00535519	3 (nicotinate and nicotinamide) m	EHMN
0.00152499	0.00535519	nidine deoxyribonucleotides <i>de	HumanCyc
0.00152499	0.00535519	Pravastatin Action Pathway	SMPDB
0.00152499	0.00535519	Atorvastatin Action Pathway	SMPDB
0.00152499	0.00535519	Rosuvastatin Action Pathway	SMPDB
0.00152499	0.00535519	Lovastatin Action Pathway	SMPDB
0.00152499	0.00535519	Cerivastatin Action Pathway	SMPDB
0.00152499	0.00535519	Fluvastatin Action Pathway	SMPDB
0.00152499	0.00535519	Simvastatin Action Pathway	SMPDB
0.00152499	0.00535519	Hyper-IgD syndrome	SMPDB
0.00152499	0.00535519	Cholesteryl ester storage disease	SMPDB
0.00152499	0.00535519	al Acid Lipase Deficiency (Wolman	SMPDB
0.00152499	0.00535519	Mevalonic aciduria	SMPDB
0.00152499	0.00535519	Wolman disease	SMPDB
0.00152499	0.00535519	Smith-Lemli-Opitz Syndrome (SLOS	SMPDB
0.00152499	0.00535519	splasia Punctata II, X Linked Domin	SMPDB
0.00152499	0.00535519	CHILD Syndrome	SMPDB
0.00152499	0.00535519	Desmosterolosis	SMPDB
0.00152499	0.00535519	Hypercholesterolemia	SMPDB
0.00152499	0.00535519	Steroid Biosynthesis	SMPDB
0.00152499	0.00535519	Alendronate Action Pathway	SMPDB
0.00152499	0.00535519	Risedronate Action Pathway	SMPDB
0.00152499	0.00535519	Pamidronate Action Pathway	SMPDB
0.00152499	0.00535519	Zoledronate Action Pathway	SMPDB
0.00152499	0.00535519	Ibandronate Action Pathway	SMPDB
0.00152499	0.00535519	todegradation of Cdh1 by Cdh1:AP	Reactome
0.00161029	0.0055684	zymosterol biosynthesis	HumanCyc

0.00161029	0.0055684	methionine degradation	HumanCyc
0.0016339	0.00560725	ion of HSF1-mediated heat shock r	Reactome
0.00172548	0.00587702	sport of Mature Transcript to Cytop	Reactome
0.00174029	0.00588321	:Cdc20 mediated degradation of S	Reactome
0.0019335	0.00648796	DNA Repair	Reactome
0.00197366	0.00657402	:Cdc20 mediated degradation of C	Reactome
0.00198881	0.00657615	Cell cycle - Homo sapiens (human)	KEGG
0.00222561	0.00719937	Methionine Cysteine metabolism	INOH
0.00223883	0.00719937	Mevalonate pathway	Wikipathways
0.00223883	0.00719937	ulatory component of the Drosha n	Wikipathways
0.00224086	0.00719937	d targets of C-MYC transcriptional a	PID
0.00242755	0.00774424	Purine metabolism	EHMN
0.00247551	0.007842	Retinoblastoma Gene in Cancer	Wikipathways
0.00249664	0.00785403	tion of gene expression by SREBF (S	Reactome
0.00260637	0.00814265	Metabolism of proteins	Reactome
0.00278723	0.00864805	f Cdc20 and other APC/C:Cdh1 targ	Reactome
0.00304574	0.00938586	Pyrimidine metabolism	EHMN
0.00309782	0.0094182	One Carbon Metabolism	Wikipathways
0.00309782	0.0094182	iated phosphorylation and remova	Reactome
0.00315926	0.00954097	Glycerophospholipid metabolism	EHMN
0.00327591	0.00982773	nediated proteolysis - Homo sapien	KEGG
0.00365369	0.01088897	Lysine metabolism	EHMN
0.00376416	0.01106269	Cellular Senescence	Reactome
0.00377488	0.01106269	Late Phase of HIV Life Cycle	Reactome
0.00378525	0.01106269	cysteine biosynthesis	HumanCyc
0.00415381	0.01206204	of cholesterol biosynthesis by SRE	Reactome
0.00459543	0.01325942	HIV Infection	Reactome
0.00464496	0.01331751	S Phase	Reactome
0.00469897	0.01338762	mevalonate pathway	HumanCyc
0.00510751	0.01446064	Infectious disease	Reactome
0.00524441	0.01475601	nscriptional regulation by small RN	Reactome
0.00540417	0.01511166	version of nucleotide di- and tripho	Reactome
0.00572011	0.01589699	ctivated Protein Kinase (AMPK) Sig	Wikipathways
0.00579512	0.01600726	Signaling by Rho GTPases	Reactome
0.00590312	0.01620674	Transcriptional Regulation by TP53	Reactome
0.00635025	0.01732929	arget Of Rapamycin (TOR) Signalin	Wikipathways
0.00679732	0.01832848	anylgeranyldiphosphate biosynthe	HumanCyc
0.00679732	0.01832848	Selenoamino Acid Metabolism	SMPDB
0.00738909	0.01980625	tRNA charging	HumanCyc
0.007978	0.02065161	cholesterol biosynthesis I	HumanCyc
0.007978	0.02065161	l biosynthesis II (via 24,25-dihydrol	HumanCyc
0.007978	0.02065161	sterol biosynthesis III (via desmost	HumanCyc
0.007978	0.02065161	Gemcitabine Action Pathway	SMPDB
0.007978	0.02065161	Gemcitabine Metabolism Pathway	SMPDB

0.007978	0.02065161	lite Pathway - Folate Cycle, Pharma	PharmGKB
0.00852269	0.02168991	eukemia virus 1 infection - Homo sa	KEGG
0.00852275	0.02168991	mTOR signalling	Reactome
0.00852275	0.02168991	Fanconi Anemia Pathway	Reactome
0.00870597	0.02196382	EGFR1	NetPath
0.00872735	0.02196382	Ub-specific processing proteases	Reactome
0.00877851	0.02197053	O E3 ligases SUMOylate target pro	Reactome
0.00924376	0.02266264	Mitotic Telophase/Cytokinesis	Reactome
0.00924376	0.02266264	gulates Transcription of DNA Repa	Wikipathways
0.00924381	0.02266264	insulin	INOH
0.00925516	0.02266264	st-translational protein modificati	Reactome
0.00948768	0.02310709	IA transport - Homo sapiens (huma	KEGG
0.00975303	0.02362633	tRNA Aminoacylation	Reactome

data Pathway enrichment analysis on the overlap between down-regulated gene

external_id	members_input_overlap
R-HSA-68886	TC1; SMC4; NUP160; NUP93; NCAPD2; NUP85
R-HSA-1640170	C1; SMC4; NBN; NUP160; NUP93; NCAPD2; NC
R-HSA-69278	C1; SMC4; NUP160; NUP93; NCAPD2; NCAPD3;
R-HSA-68877	A; NUP160; SMC2; KNTC1; NUP85; NCAPD2; SM
R-HSA-2467813	; BUB1B; CDC27; PDS5A; NUP160; KNTC1; NUP
R-HSA-68882	; BUB1B; CDC27; PDS5A; NUP160; KNTC1; NUP
R-HSA-69618	C16; BUB1B; CDC27; NUP160; KNTC1; NUP85;
R-HSA-2555396	; BUB1B; CDC27; PDS5A; NUP160; KNTC1; NUP
R-HSA-2514853	NCAPG; SMC2; SMC4; NCAPD2; NCAPH
aurora_b_pathway	N2; SMC2; SMC4; NCAPD2; NCAPH; NCAPG; KI
R-HSA-180910	AAAS; PSIP1; NUP54; NUP160; NUP93; NUP85
Aminosugars metabolism	A; NUP54; NUP160; NUP93; NUP85; MGEA5; C
R-HSA-176033	AAAS; PSIP1; NUP54; NUP160; NUP93; NUP85
lethionine and cysteine metabolis	AT2A; NUP54; NUP160; DNMT1; NUP93; NUP8
Selenoamino acid metabolism	HCYL1; NUP54; NUP160; NUP93; NUP85; MAT2
R-HSA-141430	CDC27; MAD2L1; CDC16; ANAPC7; BUB1B
R-HSA-141405	CDC27; MAD2L1; CDC16; ANAPC7; BUB1B
R-HSA-2500257	D2L1; BUB1B; PDS5A; NUP160; KNTC1; NUP85
R-HSA-69620	UB1B; CDC27; NUP160; KNTC1; NUP85; NBN;
R-HSA-6811434	KIF2A; COPB2; ARFGAP2; ZW10; KIF20A; NBAS
R-HSA-179409	CDC27; MAD2L1; CDC16; ANAPC7; BUB1B
R-HSA-141444	MAD2L1; BUB1B; NUP160; KNTC1; NUP85; ZW
R-HSA-141424	MAD2L1; BUB1B; NUP160; KNTC1; NUP85; ZW
R-HSA-174184	CDC27; MAD2L1; CDC16; ANAPC7; BUB1B
R-HSA-179419	CDC27; MAD2L1; CDC16; ANAPC7; BUB1B
R-HSA-72306	UP54; NUP160; NSUN2; NUP93; NUP85; DDX1
R-HSA-168271	NUP160; AAAS; NUP93; NUP85; NUP54
R-HSA-170822	NUP160; AAAS; NUP93; NUP85; NUP54
R-HSA-168333	NUP160; AAAS; NUP93; NUP85; NUP54
R-HSA-176409	CDC27; MAD2L1; CDC16; ANAPC7; BUB1B
R-HSA-168274	NUP160; AAAS; NUP93; NUP85; NUP54
R-HSA-176814	CDC27; MAD2L1; CDC16; ANAPC7; BUB1B
R-HSA-68875	P54; NUP160; SMC2; NUP93; NUP85; SMC4; A
R-HSA-159227	NUP160; AAAS; NUP93; NUP85; NUP54
R-HSA-165054	NUP160; AAAS; NUP93; NUP85; NUP54
R-HSA-180746	NUP160; AAAS; NUP93; NUP85; NUP54
R-HSA-159230	NUP160; AAAS; NUP93; NUP85; NUP54
R-HSA-3301854	NUP160; AAAS; NUP93; NUP85; NUP54
R-HSA-6784531	AAAS; NUP54; NUP160; NUP93; NUP85; DDX1
R-HSA-8953897	AG1; NUP160; NUP93; NUP85; CDC27; EZH2; E
R-HSA-8856688	NBAS; COPB2; ARFGAP2; ZW10; KIFC1; KIF2A;
R-HSA-176408	CDC27; MAD2L1; CDC16; ANAPC7; BUB1B

ualene and cholesterol biosynthes	NUP160; NUP93; NUP85; HMGCR; NUP54
R-HSA-4615885	NUP160; AAAS; NUP93; NUP85; NUP54
R-HSA-177243	NUP160; AAAS; NUP93; NUP85; NUP54
R-HSA-5663220	MAD2L1; BUB1B; NUP160; KNTC1; NUP85; ZW
phatidylinositol phosphate metab	C3; NUP54; NUP160; NUP93; NUP85; COPA; CO
R-HSA-159231	NUP160; AAAS; NUP93; NUP85; NUP54
R-HSA-174143	CDC27; MAD2L1; CDC16; ANAPC7; BUB1B
R-HSA-453276	CDC27; MAD2L1; CDC16; ANAPC7; BUB1B
R-HSA-159234	NUP160; AAAS; NUP93; NUP85; NUP54
R-HSA-2262752	P54; CDC27; NUP160; NUP93; NUP85; EZH2; EP
R-HSA-168325	NUP160; AAAS; NUP93; NUP85; NUP54
Glycosphingolipid metabolism	COPA; NUP54; NUP160; NUP93; NUP85; COPB2
R-HSA-70171	PP2R1B; NUP54; NUP160; NUP93; AAAS; NUP8
R-HSA-168273	NUP160; AAAS; NUP93; NUP85; NUP54
PWY-7437	OGT; MGEA5
fanconi_pathway	WDR48; USP1; NBN; FANCI; BRIP1
R-HSA-4570464	NUP160; AAAS; NUP93; NUP85; NUP54
PWY66-5	HMGCS1; LBR; HMGCR; CYP51A1
R-HSA-191273	HMGCS1; LBR; HMGCR; CYP51A1
R-HSA-199991	; COPB2; ARFGAP2; SNF8; COPS7A; TRAPPC12;
R-HSA-8953854	R1; NUP93; DIMT1; NUP85; NUP160; DDX5; DD
serine, alanine and threonine met	ARS2; NUP54; NUP160; NUP93; NUP85; AARS2
amin D3 (cholecalciferol) metaboli	NUP160; NUP93; NUP85; NUP54
R-HSA-2980766	NUP160; AAAS; NUP93; NUP85; NUP54
R-HSA-191859	NUP160; AAAS; NUP93; NUP85; NUP54
R-HSA-194441	NUP160; AAAS; NUP93; NUP85; NUP54
Pentose phosphate pathway	NUP160; NUP93; NUP85; NUP54
R-HSA-168255	NUP160; AAAS; NUP93; NUP85; NUP54
path:hsa03460	WDR48; BRIP1; MLH1; FANCI; USP1
R-HSA-5653656	; COPB2; ARFGAP2; SNF8; COPS7A; TRAPPC12;
WP2525	TYMS; DNMT1; AHCYL1; MAT2A
B5 - CoA biosynthesis from panto	NUP160; NUP93; NUP85; NUP54
din formation from dihomo gama-l	NUP160; NUP93; NUP85; NUP54
R-HSA-195258	BUB1B; NUP160; KNTC1; NUP85; PTK2; CIT; ZW
R-HSA-162909	AAAS; PSIP1; NUP54; NUP160; NUP93; NUP85
R-HSA-70326	PP2R1B; NUP54; NUP160; NUP93; AAAS; NUP8
akap95pathway	PRKAG1; DDX5; NCAPD2
WP197	HMGCS1; HMGCR; CYP51A1
R-HSA-168254	NUP160; AAAS; NUP93; NUP85; NUP54
R-HSA-3371556	RPTOR; AAAS; NUP54; NUP160; NUP93; NUP85
Glycolysis and Gluconeogenesis	NUP160; ME2; NUP93; NUP85; NUP54
WP1982	PRKAG1; HMGCS1; ACLY; HMGCR; CYP51A1
R-HSA-6811442	NBAS; COPB2; ARFGAP2; ZW10; KIFC1; KIF2A;
R-HSA-4551638	NUP160; AAAS; NUP93; NUP85; NUP54

-Inflammatory metabolites format	NUP160; NUP93; NUP85; NUP54
R-HSA-159236	NUP160; AAAS; NUP93; NUP85; NUP54
De novo fatty acid biosynthesis	NUP160; NUP93; NUP85; NUP54
Vitamin E metabolism	NUP160; NUP93; NUP85; NUP54
R-HSA-176412	CDC27; CDC16; ANAPC7
R-HSA-176407	CDC27; CDC16; ANAPC7
WP2706	HMGCS1; HMGCR; CYP51A1
SMP00214	DNMT1; MAT2A; MARS
SMP00033	DNMT1; MAT2A; MARS
SMP00221	DNMT1; MAT2A; MARS
SMP00222	DNMT1; MAT2A; MARS
SMP00341	DNMT1; MAT2A; MARS
SMP00340	DNMT1; MAT2A; MARS
SMP00570	DNMT1; MAT2A; MARS
SMP00177	DNMT1; MAT2A; MARS
R-HSA-162587	S; PSIP1; NUP54; NUP160; NUP93; PDCD6IP; NU
R-HSA-3108214	NUP160; AAAS; NUP93; NUP85; NUP54
3 (nicotinate and nicotinamide) m	NUP160; NUP93; NUP85; NUP54
PWY-7211	TYMS; DTYMK; CTPS1
SMP00089	HMGCS1; HMGCR; CYP51A1
SMP00131	HMGCS1; HMGCR; CYP51A1
SMP00092	HMGCS1; HMGCR; CYP51A1
SMP00099	HMGCS1; HMGCR; CYP51A1
SMP00111	HMGCS1; HMGCR; CYP51A1
SMP00119	HMGCS1; HMGCR; CYP51A1
SMP00082	HMGCS1; HMGCR; CYP51A1
SMP00509	HMGCS1; HMGCR; CYP51A1
SMP00508	HMGCS1; HMGCR; CYP51A1
SMP00319	HMGCS1; HMGCR; CYP51A1
SMP00510	HMGCS1; HMGCR; CYP51A1
SMP00511	HMGCS1; HMGCR; CYP51A1
SMP00389	HMGCS1; HMGCR; CYP51A1
SMP00388	HMGCS1; HMGCR; CYP51A1
SMP00387	HMGCS1; HMGCR; CYP51A1
SMP00386	HMGCS1; HMGCR; CYP51A1
SMP00209	HMGCS1; HMGCR; CYP51A1
SMP00023	HMGCS1; HMGCR; CYP51A1
SMP00095	HMGCS1; HMGCR; CYP51A1
SMP00112	HMGCS1; HMGCR; CYP51A1
SMP00117	HMGCS1; HMGCR; CYP51A1
SMP00107	HMGCS1; HMGCR; CYP51A1
SMP00079	HMGCS1; HMGCR; CYP51A1
R-HSA-174084	CDC27; CDC16; ANAPC7
PWY-6074	LBR; CYP51A1

METHIONINE-DEG1-PWY	MAT2A; AHCYL1
R-HSA-3371453	NUP160; AAAS; NUP93; NUP85; NUP54
R-HSA-72202	NUP160; AAAS; NUP93; NUP85; NUP54
R-HSA-174154	CDC27; CDC16; ANAPC7
R-HSA-73894	WDR48; USP1; MLH1; USP7; NBN; BRIP1; FAN
R-HSA-174048	CDC27; CDC16; ANAPC7
path:hsa04110	MAD2L1; CDC16; BUB1B; CDC27; CDK4; ANAPC
None	MAT2A; AHCYL1; MARS
WP3963	HMGCS1; HMGCR
WP2942	NBN; DDX1
myc_activpathway	EIF4G1; HUWE1; CDK4; NBN; TRRAP
Purine metabolism	P54; NUP160; NUP93; NUP85; ATP6V0A1; COP
WP2446	SMC2; HLTF; DNMT1; CDK4; TYMS
R-HSA-2426168	HMGCS1; HMGCR; CYP51A1
R-HSA-392499	NUP160; COPA; PSME4; NUP93; TRRAP; PIGS;
R-HSA-174178	CDC27; CDC16; ANAPC7
Pyrimidine metabolism	COPA; NUP54; NUP160; NUP93; NUP85; COPB2
WP241	TYMS; GART; DNMT1
R-HSA-69017	CDC27; CDC16; ANAPC7
Glycerophospholipid metabolism	COPA; NUP54; NUP160; NUP93; NUP85; COPB2
path:hsa04120	UBE3A; CDC16; CDC27; BIRC6; HUWE1; ANAPC
Lysine metabolism	NUP160; NUP93; NUP85; NUP54
R-HSA-2559583	DC16; CDC27; EZH2; EP400; NBN; CDK4; ANAPC
R-HSA-162599	AAS; NUP54; NUP160; NUP93; PDCD6IP; NUP8
PWY-6292	MAT2A; AHCYL1
R-HSA-1655829	HMGCS1; HMGCR; CYP51A1
R-HSA-162906	S; PSIP1; NUP54; NUP160; NUP93; PDCD6IP; NU
R-HSA-69242	CDC27; CDK4; PDS5A; CDC16; ANAPC7
PWY-922	HMGCS1; HMGCR
R-HSA-5663205	IP1; NUP54; NUP160; NUP93; PDCD6IP; NUP85
R-HSA-5578749	NUP160; AAAS; NUP93; NUP85; NUP54
R-HSA-499943	TYMS; DTYMK; CTPS1
WP1403	RPTOR; PRKAG1; PIK3C3; HMGCR
R-HSA-194315	BUB1B; NUP160; KNTC1; NUP85; PTK2; CIT; ZW
R-HSA-3700989	B; PRKAG1; MLH1; USP7; RABGGTB; NBN; CNOT
WP1471	RPTOR; PRKAG1; HMGCR
PWY-5910	HMGCS1; HMGCR
SMP00029	MAT2A; MARS
TRNA-CHARGING-PWY	AARS2; TARS2; MARS
PWY66-341	LBR; CYP51A1
PWY66-3	LBR; CYP51A1
PWY66-4	LBR; CYP51A1
SMP00446	TYMS; CTPS1
SMP00603	TYMS; CTPS1

PA165291575	TYMS; GART
path:hsa05166	2L1; CDC16; BUB1B; CDC27; TRRAP; CDK4; AN
R-HSA-165159	RPTOR; PRKAG1; EIF4G1
R-HSA-6783310	WDR48; USP1; FANCI
Pathway_EGFR1	IF4G1; HUWE1; ZFYVE16; PDCD6IP; FLOT1; TO
R-HSA-5689880	19; WDR48; PSME4; PSMD13; USP7; TRRAP; U
R-HSA-3108232	NUP160; AAAS; NUP93; NUP85; NUP54
R-HSA-68884	PDS5A; KIF20A
WP3808	MLH1; FANCI
None	RPTOR; PRKAG1; EIF4G1; PPP2R1B
R-HSA-597592	NUP160; COPA; PSME4; NUP93; TRRAP; PIGS;
path:hsa03013	AAAS; NUP54; EIF4G1; NUP93; NUP85; NUP16
R-HSA-379724	AARS2; TARS2; MARS

es (protein level) and intron retention (RNA splicing)

members_input_overlap_geneids	size
; 53371; 23397; 10051; 10112; 9688; 9735; 9183; 8881; 23310; 23244; 3796; 99	340
; 10592; 8086; 51434; 53371; 996; 4683; 1019; 9918; 64151; 3796; 23397; 1011	564
31; 23310; 701; 10592; 8086; 51434; 53371; 996; 3796; 1019; 9918; 64151; 233	481
64151; 3796; 4085; 79902; 23397; 9735; 9183; 10051; 23244; 23279; 9918; 701;	186
5519; 3796; 4085; 79902; 9735; 51434; 9183; 8881; 23244; 996; 23279; 701	129
5519; 3796; 4085; 79902; 9735; 51434; 9183; 8881; 23244; 996; 23279; 701	140
5519; 3796; 4085; 79902; 9735; 51434; 996; 9183; 8881; 23279; 701	113
5519; 3796; 4085; 79902; 9735; 51434; 9183; 8881; 23244; 996; 23279; 701	141
10051; 10592; 9918; 23397; 64151	12
10112; 9918; 10051; 23397; 64151; 10592; 54888	41
9688; 79902; 11168; 23279; 53371; 8086	32
9688; 79902; 23279; 53371; 1314; 10724; 9276	51
9688; 79902; 11168; 23279; 53371; 8086	35
9688; 79902; 23279; 1314; 53371; 4144; 1786; 9276	78
9688; 79902; 23279; 10768; 53371; 4144	36
4085; 996; 51434; 8881; 701	21
4085; 996; 51434; 8881; 701	21
9735; 5519; 3796; 4085; 79902; 9183; 23244; 23279; 701	109
519; 3796; 79902; 9735; 51434; 996; 4085; 9183; 8881; 83990; 4683; 701; 2327	250
3796; 10112; 51594; 3833; 84364; 9183; 1314; 9276	82
4085; 701; 51434; 8881; 996	26
5519; 3796; 4085; 79902; 9735; 9183; 23279; 701	96
5519; 3796; 4085; 79902; 9735; 9183; 23279; 701	96
4085; 51434; 8881; 701; 996	28
4085; 51434; 8881; 701; 996	29
1653; 79902; 63892; 53371; 9688; 23279; 8086; 54888	103
9688; 79902; 23279; 53371; 8086	30
9688; 79902; 23279; 53371; 8086	30
9688; 79902; 53371; 23279; 8086	30
4085; 51434; 8881; 701; 996	31
9688; 79902; 53371; 23279; 8086	31
4085; 51434; 8881; 701; 996	32
5519; 23310; 79902; 53371; 9688; 10051; 23279; 10592; 8086	144
9688; 79902; 23279; 53371; 8086	33
9688; 79902; 53371; 23279; 8086	33
9688; 79902; 23279; 53371; 8086	34
9688; 79902; 23279; 53371; 8086	34
9688; 79902; 23279; 53371; 8086	34
1653; 9688; 79902; 23279; 53371; 8086	57
71; 79902; 8881; 8086; 57634; 51434; 53371; 996; 4683; 1019; 9688; 23279; 21	414
1314; 3796; 9276; 10112; 3833; 9183; 51594; 84364	116
4085; 996; 51434; 8881; 701	36

3156; 9688; 23279; 53371; 79902	37
9688; 79902; 23279; 53371; 8086	37
9688; 79902; 53371; 23279; 8086	37
5519; 3796; 4085; 79902; 9735; 9183; 23279; 701	123
5289; 1314; 79902; 53371; 9276; 9688; 23279	93
9688; 79902; 23279; 53371; 8086	40
4085; 996; 51434; 8881; 701	41
4085; 996; 51434; 8881; 701	41
9688; 79902; 23279; 53371; 8086	41
902; 8881; 8086; 57634; 51434; 53371; 996; 4683; 1019; 2146; 9688; 23279; 575	345
9688; 79902; 23279; 53371; 8086	42
79902; 9688; 23279; 53371; 1314; 9276	69
79902; 9688; 5519; 23279; 53371; 8086	71
9688; 79902; 23279; 53371; 8086	44
10724; 8473	2
7398; 57599; 55215; 4683; 83990	46
9688; 79902; 53371; 23279; 8086	46
3156; 1595; 3930; 3157	25
3156; 1595; 3930; 3157	25
; 27131; 51622; 221960; 51594; 51112; 3796; 10112; 9183; 1314; 50813; 9276;	582
6; 53371; 27292; 1981; 1655; 1653; 55127; 3842; 9688; 23279; 54888; 11325; 5	586
57505; 9688; 79902; 53371; 80222; 23279	78
9688; 79902; 23279; 53371	27
9688; 79902; 53371; 23279; 8086	51
9688; 79902; 23279; 53371; 8086	52
9688; 79902; 23279; 53371; 8086	52
9688; 79902; 23279; 53371	29
9688; 79902; 23279; 53371; 8086	53
83990; 55215; 4292; 7398; 57599	54
; 27131; 51622; 221960; 51594; 51112; 3796; 10112; 50813; 9183; 1314; 9276;	620
1786; 10768; 7298; 4144	31
9688; 79902; 23279; 53371	31
9688; 79902; 23279; 53371	31
5519; 11113; 3796; 4085; 79902; 9735; 5289; 9183; 5747; 701; 23279	301
79902; 11168; 53371; 9688; 23279; 8086	89
5519; 79902; 53371; 9688; 23279; 8086	91
5571; 9918; 1655	14
1595; 3157; 3156	15
9688; 79902; 23279; 53371; 8086	63
79902; 53371; 9688; 57521; 23279; 8086	99
9688; 79902; 23279; 53371; 4200	67
3157; 1595; 47; 3156; 5571	68
1314; 3796; 9276; 10112; 3833; 9183; 51594; 84364	186
9688; 79902; 23279; 53371; 8086	70

9688; 79902; 23279; 53371	42
9688; 79902; 23279; 53371; 8086	73
9688; 79902; 53371; 23279	43
79902; 9688; 23279; 53371	43
996; 51434; 8881	20
996; 51434; 8881	20
1595; 3156; 3157	20
1786; 4141; 4144	20
1786; 4141; 4144	20
1786; 4141; 4144	20
1786; 4141; 4144	20
1786; 4141; 4144	20
1786; 4141; 4144	20
1786; 4141; 4144	20
1786; 4141; 4144	20
79902; 53371; 9688; 23279; 10015; 11168; 8086	156
9688; 23279; 53371; 79902; 8086	76
9688; 79902; 23279; 53371	47
1503; 1841; 7298	22
3156; 3157; 1595	22
3156; 3157; 1595	22
3156; 3157; 1595	22
3156; 3157; 1595	22
3156; 3157; 1595	22
3156; 3157; 1595	22
3157; 1595; 3156	22
3157; 1595; 3156	22
3157; 1595; 3156	22
3157; 1595; 3156	22
3157; 1595; 3156	22
3157; 1595; 3156	22
3157; 1595; 3156	22
3157; 1595; 3156	22
3157; 1595; 3156	22
3157; 1595; 3156	22
3157; 1595; 3156	22
3157; 1595; 3156	22
3157; 1595; 3156	22
3157; 1595; 3156	22
3157; 1595; 3156	22
3157; 1595; 3156	22
3157; 1595; 3156	22
3157; 1595; 3156	22
51434; 8881; 996	22
3930; 1595	6

10768; 4144	6
9688; 79902; 23279; 53371; 8086	81
9688; 79902; 23279; 53371; 8086	82
51434; 8881; 996	23
55183; 4292; 4683; 50813; 7398; 57599; 83990; 2873; 55215; 7874	320
51434; 8881; 996	24
8881; 701; 51434; 996; 4085; 1019	124
4141; 10768; 4144	25
3157; 3156	7
4683; 1653	7
10075; 1981; 4683; 8295; 1019	87
1314; 79902; 53371; 535; 9276; 9688; 23279; 84340	223
1786; 10592; 6596; 1019; 7298	89
3156; 1595; 3157	26
577; 94005; 50813; 2873; 9276; 4141; 8473; 1981; 23358; 23198; 10651; 9688;	2008
51434; 8881; 996	27
79902; 1314; 53371; 9276; 9688; 23279	136
1786; 2618; 7298	28
51434; 8881; 996	28
1314; 53371; 9276; 9688; 79902; 23279	136
57448; 7337; 8881; 51434; 10075; 996	137
9688; 79902; 23279; 53371	60
2146; 57634; 51434; 996; 4683; 8881; 1019	189
9688; 79902; 53371; 23279; 10015; 8086	143
10768; 4144	9
3156; 1595; 3157	31
9688; 79902; 53371; 10015; 23279; 11168; 8086	197
51434; 996; 8881; 1019; 23244	103
3156; 3157	10
9688; 79902; 53371; 10015; 8086; 23279; 11168; 84168	253
79902; 53371; 9688; 23279; 8086	107
1503; 1841; 7298	34
5289; 57521; 3156; 5571	68
5519; 4085; 79902; 9735; 5289; 701; 11113; 3796; 9183; 23279; 5747	435
5876; 5519; 4292; 5571; 7874; 4683; 83990; 55215; 4848; 57521	374
57521; 3156; 5571	36
3156; 3157	12
4144; 4141	12
57505; 4141; 80222	38
3930; 1595	13
3930; 1595	13
3930; 1595	13
7298; 1503	13
7298; 1503	13

7298; 2618	13
8295; 8881; 701; 51434; 996; 4085; 1019	219
1981; 57521; 5571	41
7398; 55215; 57599	41
10040; 10768; 27131; 10075; 1981; 9765; 50807; 5747; 84168; 10211; 10015	457
10869; 23198; 8295; 23358; 5719; 57599; 7874	220
79902; 53371; 9688; 23279; 8086	120
10112; 23244	14
55215; 4292	14
1981; 57521; 5519; 5571	78
876; 79902; 57599; 8086; 55577; 94005; 50813; 2873; 9276; 8473; 23358; 2319	1383
79902; 53371; 23279; 8086; 1981; 9688	171
57505; 4141; 80222	42

effective_size
339
563
480
186
129
140
113
141
12
41
32
51
35
78
36
21
21
109
249
82
26
96
96
28
29
103
30
30
30
31
31
32
143
33
33
34
34
34
57
413
116
36

37
37
37
123
93
40
41
41
41
344
42
69
70
44
2
46
46
25
25
582
584
78
27
51
52
52
29
53
54
620
31
31
31
300
89
90
14
15
63
99
66
68
186
70

42
73
43
43
20
20
20
20
20
20
20
20
20
20
20
154
76
47
22
22
22
22
22
22
22
22
22
22
22
22
22
22
22
22
22
22
22
22
22
22
22
22
22
22
22
22
22
22
22
6

6
81
82
23
317
24
124
25
7
7
87
222
89
26
1999
27
135
28
28
136
137
60
188
141
9
31
195
103
10
251
106
34
68
430
371
36
12
12
38
13
13
13
13
13

13
219
40
40
455
220
120
14
14
78
1378
171
42